

Development of a Novel Oral Drug Delivery System Using pH-Responsive
Hollow Microparticle with Macropores on the Surface

By

Chengmeng Sun

A thesis submitted in partial fulfillment of the requirements for the degree of

Master of Science in

Chemical Engineering

Department of Chemical and Materials Engineering

University of Alberta

© Chengmeng Sun, 2017

Abstract

Oral administration of drugs is considered advantageous over all other routes of drug delivery due to several benefits, including painless self-administration, lack of biohazardous waste, and easier and cold-chain free transportation. However, numerous environment sensitive drugs such as vaccines lose their therapeutic efficacy due to the extreme pH environment in the gastrointestinal (GI) tract. Till now, several methods have been proposed to produce microencapsulation systems for oral drug delivery, such as emulsion polymerization and spray drying. However, a universal, efficient, and effective drug delivery system for environment-sensitive biopharmaceuticals is still unavailable. The main drawback of emulsion polymerization method is the exposure of the drug to the organic solvent suspension during the microparticle synthesis process, which commonly causes loss of bioactivity of pharmaceuticals. Similarly, spray drying involves complicated optimization of the fabrication parameters such as temperature, concentrations, and feed rate for different types of drugs. To overcome these technical challenges, we have developed a novel and facile method of producing microparticles with pH-responsive macropores. And since the microparticle fabrication and drug encapsulation steps are independent, the problem of loss of bioactivity of drugs has been addressed. Microparticles were prepared using a FDA approved pH-responsive copolymer poly-(methacrylic acid-*co*-ethyl acrylate) with a monomer ratio of 1:1. Scanning electron microscopy analysis was used to study morphology and confirm the pore formation. The microparticles were sized $\sim 35 \mu\text{m}$ in diameter with pores' diameter

ranging from 1-10 μm . In a systematic approach, the effects of stirring, temperature, and evaporation time on pore formation were investigated. Following successful encapsulation of model drug (100 nm fluorescent nanoparticles, abbreviated as FNPs) and pH-sensitive drug (pravastatin sodium), the release profiles of ingredients were studied by employing UV-Vis, UV-MS, and fluorescence microscopy to demonstrate our proof-of-concept intestine-targeted drug delivery system. In this work, we found that the encapsulated pravastatin maintained $> 60\%$ of its original activity and was released after 6 hours of incubation in simulated GI tract environment which proved that the high effectiveness of our proof-of-concept microparticles drug delivery system.

Acknowledgements

I would first like to thank my supervisor, Dr. Hyo-Jick Choi, and co-supervisor, Dr. Carlo Montemagno, both of the Chemical and Material Engineering Department at the University of Alberta. Without their patient guidance, advice, and help, I could never have finished my thesis. From the beginning of my MSc study, they had been strict with me about researching the literature, experimental work, and maintaining good habits in summarizing my research, which have turned out to be the best strategies that not only have helped with my thesis, but will also benefit my whole life.

I would also like to thank Ingenuity Lab, which is the best platform research I have ever seen. All the colleagues, students, and staff members are knowledgeable and are always willing to help. Here, we have the collaboration of the best people with the best equipment.

I would also like to thank my lab members, Ankit Kumar, Bahman Homayun and Ilaria Rubino. They have been supportive of both my thesis work and my daily life. Ankit provided specific guidance about many instrumental techniques. Bahman helped me with the SEM analysis. Ilaria solved many problems with my academic writing. I am very proud to have them not only as my colleagues but also as my friends.

Finally, I must express my very profound gratitude to my parents and my sister for providing me with unfailing support and continuous encouragement.

Table of Contents

1	Introduction.....	1
1.1	Drug delivery systems and macromolecular drugs	1
1.2	Microparticle fabrication techniques for applications in oral drug delivery	3
1.3	pH-responsive microparticles.....	8
1.4	Fabrication of proof-of-concept smart microparticles and determination of release profile	9
1.5	Scope of work.....	10
2	Materials and Methods.....	12
2.1	Materials.....	12
2.2	Fabrication of microparticles with macropore	13
2.2.1	The effects of stirring and steady evaporation temperature on microparticles.....	13
2.2.2	Pore closure by freeze-drying	14
2.3	Encapsulation and release behavior of FNPs	15
2.3.1	FNPs encapsulation conditions	15
2.3.2	FNPs release.....	16
2.4	Pravastatin encapsulation and controlled-release profile study	17
2.4.1	Pravastatin sodium stability test and acquisition of its calibration curve	17
2.4.2	Pravastatin encapsulation and release conditions	18

2.5	Characterization methods.....	19
2.5.1	Scanning electron microscopy (SEM)	19
2.5.2	Fluorescence Microscope.....	20
2.5.3	High-performance liquid chromatography-mass spectroscopy (HPLC-MS)	20
2.5.4	High-performance liquid chromatography—UV/Vis (HPLC-UV/Vis) ..	21
2.5.5	Proton nuclear magnetic resonance (¹ H NMR)	21
2.6	Statistics	22
3	Results and Discussion	23
3.1	Development of pored L100-55 microparticles	23
3.2	Effect of process parameters on pore formation and pore closure process	24
3.2.1	Effect of stirring and evaporation temperature on microparticles and pore closure process	24
3.2.2	Effect of rotated evaporation duration on microparticles and pore closure process.....	30
3.3	FNPs encapsulation and visualization of release behavior	32
3.4	Encapsulation of Pravastatin and its release profile.....	35
3.4.1	Time-dependent pH responsiveness of pravastatin encapsulated microparticles by SEM imaging	35
3.4.2	Pravastatin release profile	39
3.5	Pore formation mechanism exploration	47
4	Conclusion and Future Work	53
	References.....	56

List of Figures

Figure 1 Schematic representation of 1) solid microparticles, and 2) microcapsules. Adapted from [23].....	4
Figure 2 Schematic representation of Eudragit pH-responsive pored microparticle delivery system [39].....	6
Figure 3 Chemical structures of Eudragit L100-55 (x:y=1:1, n≈120) (left) and Eudragit S100 (x:y=1:2, n≈80) (right)	7
Figure 4 Chemical structure of pravastatin sodium (left) and its 3-alpha isomer (right)	10
Figure 5 SEM images of 120 min sample	24
Figure 6 Histogram of sample pore/microparticles size ratio with sample fabrication conditions of a) original L100-55 polymer; b) evaporation at 65°C, then 37°C; c) 37°C overnight; and d) stirred at room temperature	25
Figure 7 Histogram of pored microparticles/total microparticles number ratio with sample fabrications condition of a) original L100-55 polymer; b) evaporation at 65°C, then 37°C; c) 37°C overnight; and d) stirred at room temperature.....	26
Figure 8 Histogram of pore/microparticles size ratio for freeze-dried with sample fabrication conditions of a) original L100-55 polymer; b) evaporation at 65°C, then 37°C; c) 37°C overnight; and d) stirred at room temperature	28
Figure 9 Histogram of pored microparticles/total microparticles number ratio for freeze- dried with fabrication conditions of a) original L100-55 polymer; b) evaporation at	

65°C, then 37°C; c) 37°C overnight; and d) stirred at room temperature.....	29
Figure 10 Histogram of pore/microparticles size ratio for microparticles prepared with rotated evaporation duration of a) 0 min; b) 15 min; c) 30 min; d) 60 min; or e) 120 min.....	31
Figure 11 Fluorescence microscope images of FNP encapsulated microparticles in pH 2.0 buffer with incubation time a) 0 min; b) 10 min; c) 20 min; d) 30 min; e) 60 min; f) 90 min; or g) 120 min.....	33
Figure 12 Fluorescence microscope images of FNP encapsulated microparticles in pH 7.1 buffer with incubation time a) 0 min; b) 10 min; c) 20 min; d) 30 min; e) 40 min; f) 50 min; g) 60 min; h) 240 min; i) 1000 times diluted FNPs stock solution in pH 7.1 buffer; a	34
Figure 13 SEM images of pravastatin sodium encapsulated microparticles in pH 2.0 buffer	37
Figure 14 SEM images of pravastatin sodium encapsulated microparticles in pH 7.1 buffer	38
Figure 15 HPLC-MS spectrum of pravastatin encapsulated microparticles after 6 hours incubation in simulated GI tract pH	40
Figure 16 HPLC-UV spectrum of 20 µg/mL pravastatin sodium in pH 7.1 buffer at 0 min.....	41
Figure 17 HPLC-UV spectrum of 20 µg/mL pravastatin sodium incubated at 37°C and pH 2.0 environment for 15 min.....	41
Figure 18 HPLC-UV calibration curve of Pravastatin sodium in pH 7.1 buffer with	

concentration ranging from 10-50 $\mu\text{g/mL}$ and step size of 10 $\mu\text{g/mL}$	42
Figure 19 HPLC-UV calibration curve of Pravastatin sodium in pH 7.1 buffer with concentration ranging from 2-10 $\mu\text{g/mL}$ and step size of 2 $\mu\text{g/mL}$	43
Figure 20 HPLC-UV peak integral of pravastatin sodium encapsulated microparticles in response of incubation time in GI tract pH, (PRA total: the peak integral of pravastatin sodium encapsulated microparticles with pH 7.1 applied from the start of incubation follo	45
Figure 21 HPLC-UV peak integral of pravastatin sodium incubated in simulated GI tract pH without microparticles, as the control group	46
Figure 22 ^1H NMR spectrum of the L100-55 polymer in CD_3OD	48
Figure 23 ^1H NMR spectrum of DCM supernatant of 0 min rotated evaporation sample in CD_3OD with 10mM DMSO as a reference	49
Figure 24 Schematic representation of Polysorbate 80 chemical structure and ^1H NMR proton positions	49
Figure 25 Chemical structure of sodium lauryl sulfate [57]	52

1 Introduction

1.1 Drug delivery systems and macromolecular drugs

A formulation or a device that introduces a therapeutic substance in the body and improves its effectiveness and safety by controlling the rate, endurance, and place of release of drugs, is referred to as a drug delivery system [1]. Drug delivery systems can be categorized by their routes of delivery as oral, intravenous, intramuscular/subcutaneous, transdermal, transnasal, and pulmonary delivery [2, 3]. Majority of the macromolecular drugs such as the therapeutic peptides, proteins, oligosaccharides, nucleic acids, and most of the vaccines are mainly administered intramuscularly/subcutaneously through injections. However, injection method has raised concerns of poor patient compliance, and biohazard management from used needles [4]. In addition, requirements of trained medical personnel and cold-chain storage for injectable drugs such as vaccines has elevated economic concerns and convenient applicability in poor countries, especially during epidemic/pandemic scenarios. These concerns have led to exploration of alternative delivery systems for biotherapeutics. In this context, oral delivery has attracted major research interest in the scientific community because it offers major advantages such as self-

administration and convenient solid formulation with higher stability and better safety [5]. Importantly, the route of administration is critical in triggering immune responses at the site where pathogens invade the host [6]. For some pathogens, systemic vaccination produces large amount of neutralizing antibodies. These antibodies enter the tissue parenchyma or the mucosal lumen, undergo opsonisations with the pathogens, and finish the clearance [7, 8]. Other pathogens may induce chronic infections, such as HIV, herpes virus, mycobacteria and parasitic infections [9]. In these cases, stimulating antibodies alone and systemic T-cell response may not be sufficient. Local induction of the mucosal innate and adaptive immune response, including T-helper (Th)1-, Th2-, cytotoxic CD8 T-cells, IgA and IgG₁ antibodies may also be required for a complete immune response against invasive pathogens [10]. Therefore, much efforts have been dedicated to develop mucosal vaccines. Most pathogens enter mucosal routes through nose, lungs, and the gastrointestinal (GI) tract [11]. Micro folded M-cells, which lie in Peyer's patch of small intestine, play a significant role in stimulating mucosal immunity and in absorption of macromolecules by paracellular and transcellular transport [12]. As such, oral administration has significant advantage over other routes the availability of large mucosal surface area and absorption sites. Due to these factors, more than 80% of the most popular pharmaceutical products in the US and European markets are given orally [13].

Although oral delivery has many advantages, it also has inherent difficulties and barriers. Especially, the harsh acidic conditions and enzymatic denaturation of sensitive bio-macromolecules in GI environment represent the main technical

challenges [14, 15]. During the past few decades, scientists have successfully developed various methods to stabilize macromolecular drugs for oral delivery, by utilizing PEGylation, glycoengineering, and acylation [16-18]. At the same time, microfabrication technologies utilizing biodegradable materials such as PLGA, PLA, PCL, and chitosan have been developed as adjuvants to generate solid formulation of these drugs. [19-22]. However, the lack of compatible and efficient delivery carriers, and their fabrication technologies have greatly limited the adaptability of these methods in commercial applications.

1.2 Microparticle fabrication techniques for applications in oral drug delivery

Microparticles can be mainly categorized into: 1) solid microparticles, which are micron-sized solid spherical particles with drug molecules uniformly dispersed in the polymer matrix; and 2) microcapsules, which are microparticles with empty interior spaces, where drug ingredients can be encapsulated (Figure 1) [23, 24]. Many methods for fabricating solid microparticles and microcapsules have been developed for oral drug delivery during the past few decades, including emulsion-solvent evaporation/extraction, phase separation, and spray-drying, etc. Emulsion-solvent

evaporation/extraction is reported to be the most widely employed method to prepare microparticles [25]. By dispersing small droplets of one liquid phase into the other

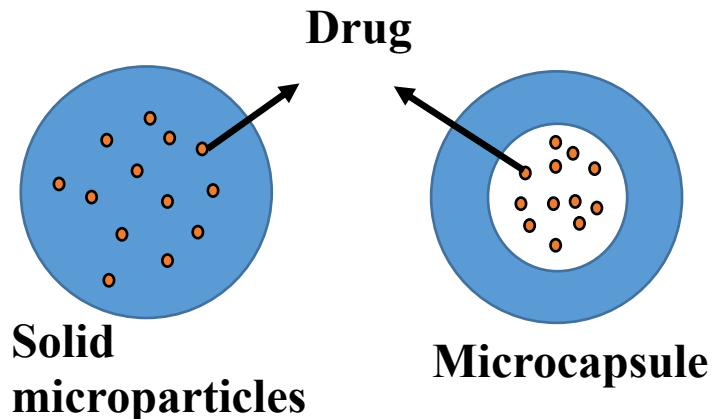


Figure 1 Schematic representation of 1) solid microparticles, and 2) microcapsules. Adapted from [23]

immiscible liquid phase, emulsion is formed. Emulsion can be stabilized with the proper use of emulsifier reagents. It can be divided into two methods, single emulsion and double emulsion. For single emulsion, polymers are dissolved by selected organic solvent and the mixture is dispersed into either mineral oil (o/o) or aqueous solution (o/w) containing drugs [26]. After emulsion is formed, organic solvent can be removed by either leaching volatile organic solvent in the dispersed phase (solvent evaporation) or by transferring the emulsion to a quenching medium (solvent extraction) to finish the solidification of microparticles [27]. Phase separation method is another method which is reported to generate drug encapsulated microparticles. The key concept is to add a solvent which is miscible with the good solvent containing the selected drug and polymer, but does not dissolve the polymer [28, 29]. By slowly adding the non-solvent,

the polymer is then concentrated and induced to phase separation with formation of coacervate droplets that contain the drug [30]. However, the use of toxic organic solvent during fabrication procedure raises safety concerns [31]. Importantly, the native secondary and tertiary structures of therapeutic proteins and peptides are maintained by relatively weak noncovalent forces. And, exposure to organic solvents can disrupt these forces and lead to diminished substrate binding and catalytic turnover [32, 33]. For example, fluorescence intensity and emission wavelength of chymotrypsin can be sharply changed toward those of free tryptophan after addition of 40% 2, 3-butanediol to its aqueous buffer [34]. Spray-drying is another method for producing fine microparticles, while lowering the exposure duration of drug to organic solvents [35]. In a typical procedure, air or drug solution is injected to small polymeric droplets to make emulsion. After that, the emulsion is sprayed into the outer drying chamber. The organic solvent can be fast evaporated due to the large surface area/volume ratio of the small spray droplets [36]. Spray-drying has been widely employed for microparticles preparation. However, this method is also faced with a limitation in the general application depending on the polymer type and drug combination (e.g., feed material properties, concentration of drugs and polymers, feed rate, and inlet/outlet temperatures) [37]. In addition, the attachment of the polymer to the inner wall of the drying chamber may result in loss of a considerable amount of the drugs and materials [38].

To overcome the described barriers, Kumar et al. in our group developed smart hollow microparticles with pH-responsive (see section 1.3) macropore on their surface. The

microparticles were fabricated utilizing a pH-sensitive PMMA-PMAA (methacrylic acid: methyl methacrylate copolymer = 1:2, Eudragit S100) copolymer using O/W emulsion with a critical co-solvent system [39]. The pored microparticles can be loaded with the desired drug molecules in a separate encapsulation step. To protect the drug from the harsh GI tract environments, pore closure is a critical process in pored microparticles delivery systems. Kumar et al. proposed a first-of-its-kind pore sealing method for pH-responsive microparticles by precise freeze-drying of pored microparticles dispersed in water [39]. After completion of pore closure, microparticles protected the therapeutic ingredients by keeping the pores closed in the acidic gastric fluid. And, microparticles rapidly opened their pores or dissolved in the intestinal pH environment to release the encapsulated drugs [39].

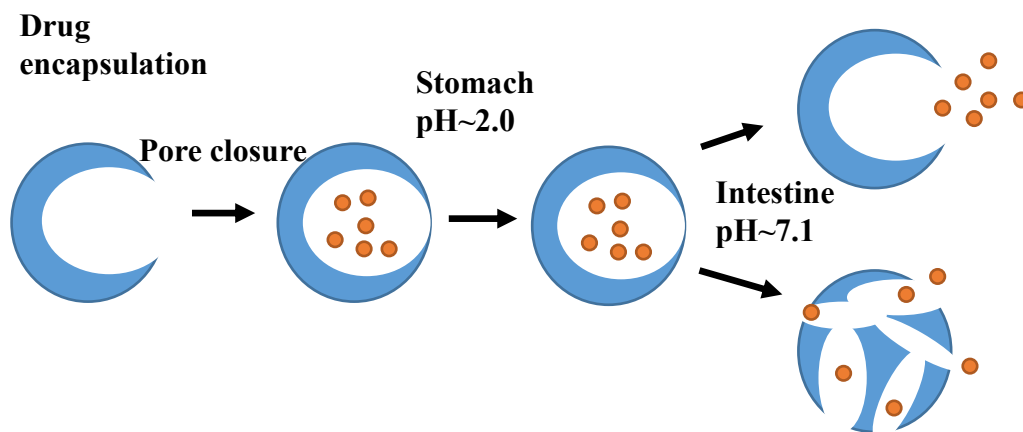


Figure 2 Schematic representation of Eudragit pH-responsive pored microparticle delivery system [39]

In our approach, methacrylic acid and ethyl acrylate copolymer (1:1, Eudragit L100-55, $pK_a \approx 5.4$) was selected because of its lower pK_a compared to S100 ($pK_a \approx 6.8$) (Figure 3). Therefore, L100-55 swells at $pH > 5.5$ compared to $pH \geq 7.0$ for S100 [40]. Hence, L100-55 was expected to have more thorough dissolution at intestinal pH. However, there was difficulty in establishing a co-solvent system for the L100-55 copolymer. The yield of smart microparticles (30 – 40 mg microparticles/6 liters emulsion) also needed improvement. Kumar et al. have characterized the release profile of model drugs using fluorescence nanoparticles (FNPs) and fluorescent dye encapsulation [39]. In this study, the microparticles' capability to protect drugs from the stomach's harsh pH environment is further investigated by encapsulating real drugs. Therefore, this study aims to develop an alternative method for developing smart microparticles drug delivery system and test its performance with real drugs.

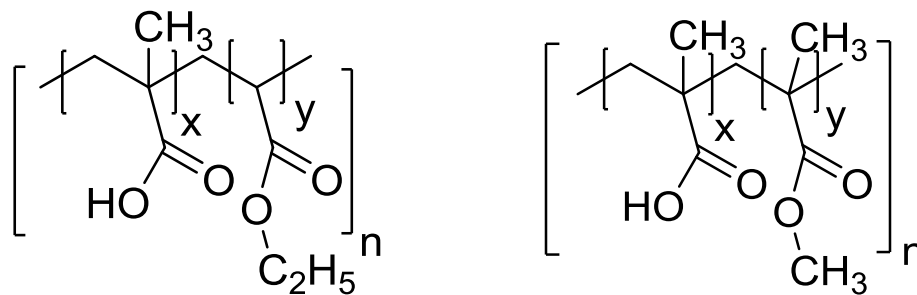


Figure 3 Chemical structures of Eudragit L100-55 ($x:y=1:1$, $n \approx 120$) (left) and Eudragit S100 ($x:y=1:2$, $n \approx 80$) (right)

1.3 pH-responsive polymers

Generally, pH-sensitive polymers consist of pendant acidic or basic groups that can either be protonated or deprotonated in response to changes in environmental pH [41]. Polymers with large number of these ionisable groups, are referred to as polyelectrolytes, and can be broadly classified into two types: polyacids and polybases. Poly-(acrylic acid) (PAA) and poly-(methacrylic acid) are commonly used as pH-responsive polyacids [42, 43]. When the environmental pH reaches the pKa of their pendant acidic groups, these groups undergo ionisation and rapidly change the net charge of the attached groups, subsequently inducing alteration in molecular structure of the polymer chains. By manipulating the monomers and their ratios, pKa and pH responsiveness can be designed considering target-specific pH requirement [44, 45]. Ideally, for GI tract delivery targeting small intestine, the pKa of pH responsive polymer should be well above the pH of gastric fluid to maintain intact structure, and below the environmental pH of small intestine to show responsiveness.

1.4 Fabrication of proof-of-concept smart microparticles and determination of release profile

In this experiment, instead of using micro-emulsion method, only a single organic solvent – dichloromethane (DCM) was employed. Through proper contact duration, DCM diffuses into the polymer matrix and swells the original microparticles. Later, by controlling solvent evaporation, pores are formed and enlarged with increased interior space. Hence, the parameters related to solvent evaporation became critical for controlling the pores. It has been reported that size and number of pores on microparticles can be affected by the removal rate of organic solvent at the evaporation step [46]. Although the mechanism behind this phenomenon has not been clearly identified yet, the reason may be that lower evaporation rate allows more time for a non-solvent to uniformly diffuse and swell the microparticles, which is likely to create a smoother and more regular-shaped interior space. Thus, the gentle evaporation of the solvent is more likely to create a single macropore on the surface rather than multiple small pores [46]. Also, slower solvent evaporation rate may avoid creating multiple pores or broken fragments induced by burst evaporation.

In this study, 100 nm fluorescent nanoparticles were chosen to mimic the average-sized macromolecular drugs, such as vaccines. Additionally, pravastatin was selected as a pH-sensitive drug to demonstrate the effectiveness of our drug delivery system. Pravastatin is a HMG-CoA (3-hydroxy-3-methylglutaryl-coenzyme A) reductase

inhibitor (see Figure 4) [47]. Specifically, pravastatin is known to lower the plasma low-density lipoprotein (LDL)-cholesterol level and inhibit the rate-limiting step of cholesterol synthesis in the liver by increasing hepatic LDL receptor activity. It is also used to lower cholesterol and triglycerides (types of fat) in the blood [48, 49]. The desired metabolism sites of pravastatin sodium are the liver and small intestine [50]. Pravastatin is unstable at acidic pH, and its main metabolite in an acidic environment is 3- α -iso-pravastatin, which maintains only 1/10 to 1/5 of its original therapeutic bioactivity [51]. Previously, HPLC-UV and HPLC-MS methods have been employed to determine and quantify the release behavior of pravastatin [52-54].

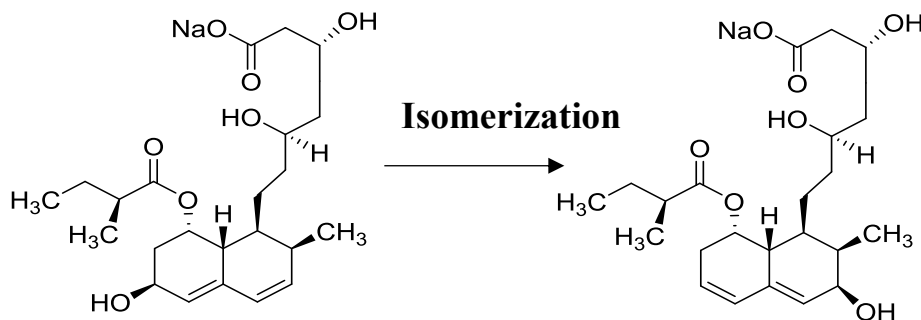


Figure 4 Chemical structure of pravastatin sodium (left) and its 3- α isomer (right)

1.5 Scope of work

This research aims to develop a new ‘emulsion-free’ method of fabricating microparticles, utilizing Eudragit L100-55 polymer with pH-responsive pores. The key idea is that drug-encapsulating microparticles should keep the pores closed to protect

drugs from the acidic stomach environment and release the drugs in the neutral environment of small intestine through pores opening. Finally, the viability of the proposed drug delivery system should be tested using both selected model drug: FNP, and real drug: Pravastatin Sodium. To achieve the outlined goal, the entire project was divided into several sub-goals:

- 1) To fabricate microparticles with pH-responsive macropores using L100-55 polymer, and evaluate the successfulness of the pore formation
- 2) To confirm the pore size controllability by changing fabrication parameters
- 3) To demonstrate pH-dependent release/protection behavior by model and real drugs encapsulation and release experiments
- 4) To study the pore formation mechanism

2 Materials and Methods

2.1 Materials

EUDRAGIT[®] L 100-55 polymer was received as a generous gift from Evonik Canada Inc. (Burlington, Ontario, Canada). For all the water requirement, 0.2 μm filtered deionized (DI) water was used. Pravastatin sodium salt hydrate was purchased from Sigma-Aldrich (St Louis, Missouri, USA), and dichloromethane, which was used for microparticles fabrication, was obtained from Fisher Scientific (Mississauga, ON). A benchtop centrifuge (Eppendorf[™] Model 5810) was used with an Eppendorf 5430/R rotor for concentration and separation of microparticles, and a Büchi[®] R200 rotary evaporator was used for homogenous evaporation of the solvent. An AdVantage Pro Freeze Dryer (SP scientific, USA) was used for pore closure purpose. Fluorescent nanoparticles (FNPs; FluoSpheres[®] Carboxylate Microspheres, 0.1 μm) were obtained from Life Technologies. HPLC mobile phase reagents, sodium dodecyl sulfate, acetonitrile, and disodium hydrogen phosphate were purchased from Sigma-Aldrich. Methanol- d^4 , poly (methyl acrylate-*co*-meth acrylic acid) (PAA-*co*-PMMA) and polysorbate 80 (abbreviated as Polysorbate 80) were also purchased from Sigma-Aldrich for ¹H-NMR experiments.

2.2 Fabrication of microparticles with macropore

In a typical synthesis process, 5 g of the EUDRAGIT® L 100-55 polymer was dispersed into 100 mL DCM (dichloromethane) kept in a 250 mL round bottom flask and vortexed for 2 min. Then the mixture was rotated at 50-60 RPM in a rotary evaporator with liquid nitrogen as the cooling agent for 120 min. Later, 10 mL of this mixture was added to 250 mL petri-dishes in quintuplicate. Then, the samples were transferred and dried in 65°C incubator for 30 min, followed by overnight incubation at 37°C. The microparticles sample was collected and used for further analysis.

2.2.1 The effects of stirring and steady evaporation temperature on microparticles

Regarding the effect of stirring, 5 g of our polymer were added to a 100 mL DCM in a beaker and then vortexed for 4-5s. Then the mixture was stirred at room temperature overnight. After overnight incubation, the sample powder was collected for further SEM analysis, FNP encapsulation and fluorescence microscopy imaging. Regarding the effect of incubation temperature, 5 g of L100-55 were mixed with 100 mL DCM. Then, the mixture was vortexed for 4-5s. Then 10 mL of the mixture were put into 250 mL petri-dishes. The containers were moved into 65°C for 30 min, then 37°C overnight and directly 37°C overnight, respectively.

To study the effect of rotated evaporation duration on pore formation process, samples

with different rotary times were prepared in 0 min, 30 min, 60 min and 120 min, with all other sample preparation conditions as described in the general techniques section.

2.2.2 Pore closure by freeze-drying

Pore closure was achieved by employing a modified freeze-drying method developed by Kumar et al. Drying duration of previous freeze-drying pore sealing protocol was increased by 1,000 min for Eudragit L100-55 microparticles to ensure sufficient drying, because of the larger size and higher concentration. Initially, 100 mg of microparticles powder suspension in 1 mL DI water was prepared in a 2 mL Eppendorf tube. Then the tube was vortexed for 4-5 s and quickly frozen in liquid nitrogen [39]. The frozen microparticles sample was transferred to the freeze-dryer (pre-cooled to -40°C) and freeze-dried according to the recipe described in Table 2-1. After the completion of the drying process, sample was stored at 4°C until use.

Table 2.1: Recipe for freeze-drying (Modified from Kumar's work [39])

Step	Shelf (°C)	Ramp (min)	Hold (min)	Vacuum (mTorr)
Low temp Drying				
1	-40	0	30	1000
2	-55	60	1	100
3	-55	0	3000	100
High temp Drying				
4	30	180	120	300

2.3 Encapsulation and release behavior of FNPs

2.3.1 FNPs encapsulation conditions

40 mg of microparticles sample was mixed with five-fold diluted FNP solution, followed by vortex for 30 s in a 2 mL Eppendorf tube. To encapsulate FNPs, 4-5 times of on-off cycle of the vacuum was applied until no air bubbles were observed from the sample. The tube was centrifuged at 500 RCF for 2 min to remove the non-encapsulated FNP. After removing supernatant, 1 mL of DI water was added to resuspend the pellet. Then, the suspension was quickly vortexed for 1-2 s, followed by freezing in liquid nitrogen. The frozen sample was freeze-dried as described in the section 2.2.2.

2.3.2 FNPs release

To create the simulated gastrointestinal pH environment for controlled-release test of microparticles, acidic (gastric pH: 2.0) and neutral (intestinal pH: 7.1) conditions must be prepared. Therefore, two types of buffers, acidic and basic, were prepared. pH 2.0 acidic buffer was prepared with potassium chloride (KCl) and hydrochloric acid (HCl). Specifically, 0.1 wt% KCl solution was stirred on a magnetic stirrer plate. Then 0.1 wt% HCl was added dropwise to adjust the final pH to 2.0. The basic buffer was 0.1 wt% disodium phosphate (Na_2HPO_4). pH 7.1 buffer was acquired by mixing acidic buffer with basic buffer in a ratio of 1:3.5 (v/v).

Upon completion of freeze-drying of FNP encapsulated microparticles, samples were collected. Then 1 mL of pH 2.0 acidic buffer was added into the sample tube, and the mixture was vortexed for 2 min to remove the FNPs attached to the outer layer of microparticles and FNPs that were encapsulated into microparticles, but were with open pores. To separate the supernatant and the microparticles, the mixture was centrifuged at 500 RCF for 1 min. Then the supernatant was carefully removed using 1 mL and 100 μL micro-pipettes. After removal of the supernatant, the sample was suspended with 1 mL of pH 2.0 solution and incubated for 2 hours to simulate the gastric environment. After that, 3.5 times the volume of the acidic addition was added to each tube to simulate the intestinal environment. At each time interval, the incubated solution was taken out for fluorescence microscopy imaging. The detailed volume and settings of the fluorescence microscope are described in section 2.5. Microparticles

sample without FNPs encapsulated and 1000 times diluted FNP solution were used as the blank group and the control group.

2.4 Pravastatin encapsulation and controlled-release profile study

2.4.1 Pravastatin sodium stability test and acquisition of its calibration curve

To determine the stability of pravastatin in the test conditions over time, 0.05 mg, 0.1 mg, 0.2 mg, 0.5 mg, and 1 mg of pravastatin were suspended with both DI water and pH 7.1 solution (acidic buffer: basic buffer = 1:3.5). The solutions were incubated at room temperature for 12 hours. HPLC-UV was performed on those solutions for both before and after incubation.

For acquisition of pravastatin sodium calibration curve, a set of 10 to 50 $\mu\text{g/mL}$ pravastatin sodium in pH 7.1 solution with a step size of 10 $\mu\text{g/mL}$, was prepared. Another set of 2 to 10 $\mu\text{g/mL}$ pravastatin sodium in pH 7.1 solution with a step size of 2 $\mu\text{g/mL}$, was prepared. To subtract other chemical signals in the matrix, HPLC-UV signal from pH 7.1 solution was also obtained. Solution preparation and HPLC-UV test were performed in triplicate for all concentrations to acquire pravastatin calibration curve.

2.4.2 Pravastatin encapsulation and release conditions

25 mg of pravastatin sodium powder was dissolved into 5 mL of DI water. Later, pH 2.0 acidic buffer was added dropwise to the suspension to adjust the final pH of the solution to pH = 5.04, which was approximately the pH of the DI water used. After the preparation of the pravastatin stock solution, 40 mg of microparticles sample (120 min time condition) was suspended with 1 mL of pravastatin stock solution in a 2 mL tube, and was followed by the same vacuum cycles and freeze-drying conditions described in section 2.3.1. After freeze-drying, the samples were collected and stored in 4°C refrigerator for further release tests.

Pre-washing steps before release were performed as described in section 2.3.2. After washing, a sample pellet was suspended with 4 mL of pH 2.0 acidic buffer in a 15 mL Eppendorf tube. Slow shaking was applied to the sample in 37°C water bath for 2 hours. During this process, for every 30 min, 250 µL sample solution was moved to a 1.5 mL tube. The sample was centrifuged at 5000 RCF for 2 min. Then the supernatant was taken out using a micro-pipette and filtered by a 0.2 µm Rc (Corning, Inc., Germany) syringe top filter with the help of a 1mL plastic syringe. After that, 100 µL of the filtrate was mixed with 350 µL of the basic buffer in another 1.5 mL tube for HPLC-UV and HPLC-MS tests. At the beginning of acidic incubation, another 250 µL of sample were taken out apart from 0 min sample into a 1.5 mL tube, 875 µL of basic buffer was added to the tube, and it was treated under the same shaking and water bath

conditions as the 15 mL tube for the whole 6 hours incubation process as an indication of the maximum encapsulated pravastatin sodium. After 2 hours acidic incubation, 8.75 mL of basic buffer were added to the 15 mL tube. Then the sample solution was further incubated for 4 hours. Every 30 min, 1 mL of the sample solution was taken out following the same centrifugation and filtration steps. Without further adding basic buffer, the filtrate was collected for HPLC-UV and HPLC-MS. Also, 40 mg of 120 min sample microparticles without pravastatin encapsulated as background group were mixed with 4 mL acidic buffer and 14 mL of basic buffer following the same incubation, centrifugation, and filtration steps.

2.5 Characterization methods

2.5.1 Scanning Electron Microscopy (SEM)

Field Emission S4800 Electron Microscope (Hitachi, Japan) was utilized for observation of morphology of synthesized microparticles, freeze-dried microparticles and their pH responsiveness during the release process. In a typical procedure, microparticles in the powder form were placed uniformly on a double-sided carbon tape, fixed to an aluminum stub. The sample was coated with a 7 nm gold layer to minimize the charging effect. The observation was performed at 15 kV (20 μ A). For pH responsiveness observation during the release testing, at each time interval, 40 μ L of the sample solution was placed on a glass coverslip, attached to a double-sided

carbon tape and fixed onto an aluminum stub. Then the major portion of the water was quickly removed by blotting using a filter paper, and the sample was further dried by employing vacuum force in the vacuum oven.

2.5.2 Fluorescence Microscope

An Olympus IX81 inverted microscope (Olympus, Germany), coupled with a DP 80 digital camera and dual CCD sensor, was used for the fluorescence microscopy analysis. The software used for obtaining micrographs was CellSens (Olympus, Germany). The images were captured at 40X objective (Olympus LCPlanFl, 1 μm depth of field, NA 0.6). Sample solutions obtained from the release test at different time intervals were placed on a glass slide and imaged under FITC mode after covering with a glass coverslip.

2.5.3 High-performance Liquid Chromatography-Mass Spectroscopy (HPLC-MS)

To confirm the presence of pravastatin and its 3 α -isoform, Agilent 1100 series with LC/MSD detection was employed. The experiment was performed in the positive mode with a scan range of 100-800 m/q. The column used was Zorbax SB-C18, 5 μm , 4.6x250 mm, which was purchased from Agilent Technologies, Inc., with 0.1 wt% formic acid (Sigma-Aldrich) in a mixture of DI water and acetone nitrile, 3:1 (v/v), as its mobile phase. The flow rate was set to 0.5 mL/min, and the pump time for each

measurement was set to 10 min. Samples were injected with 20 μL scale. HPLC-MS tests were performed on pravastatin encapsulated in 120 min rotated evaporated L100 microparticles, which were incubated for 6 hours in simulated GI tract pH. Also, 50 $\mu\text{g}/\text{mL}$ pravastatin sodium in pH 7.1 buffer was tested as the control group. pH 7.1 buffer with microparticles was tested as the blank group.

2.5.4 High-performance Liquid Chromatography—UV/Vis (HPLC-UV/Vis)

HPLC-UV/Vis was performed using Agilent 1100 series with the same column as HPLC-MS test. 25 mM of Na_2HPO_4 with 1 mM of Sodium dodecyl sulfate were dissolved in DI water and then mixed with acetonitrile (aqueous: acetonitrile (v/v) = 3:1) as the HPLC mobile phase. The flow rate was set to 1 mL/min, and the pump time for each measurement was set to 10 min. Samples were injected with 20 μL scale. The detection wavelength was set to 238 nm with a reference of 100, 600 nm. Testing of release samples from each time point was performed in triplicate.

2.5.5 Proton Nuclear Magnetic Resonance (^1H NMR)

To understand the mechanism of pore formation, dissolution of L100-55 polymer in dichloromethane was tested using a 500 MHz Varian NMR spectrometer with VnmrJ 2.2c as the analyzing software. For sample preparation, L100-55 polymer was dispersed in DCM, followed by rotary evaporation for different time intervals (0 min,

15 min, 30 min, 60 min, and 120 min) as described in the section 2.2.1. After rotated evaporation, the mixture was filtered two times with 0.2 μm regenerated cellulose syringe top filters (Corning Inc., Germany). The filtered DCM was collected and evaporated under the same conditions described in the section 2.2.1. Then, the remaining product was re-suspended in 2mL of methanol- d_4 to obtain ^1H NMR samples. To further confirm the inducement of ^1H NMR peak integral variation, Polysorbate 80 and PAA-*co*-PMMA were also treated with the same sample preparation process followed by the ^1H NMR test. To quantitatively analyze the peak intensity, 10 mM of dimethyl sulfoxide- d_6 (DMSO- d_6) was added to each ^1H NMR sample as a reference.

2.6 Statistics

Data were analyzed using student's t-test or analysis of variance (ANOVA) in Origin 2016 software (OriginLab Corporation, Northampton, MA, USA). P values calculated as less than 0.05 indicated significant differences.

3 Results and Discussion

3.1 Development of pored L100-55 microparticles

Several researchers have reported methods of fabricating microparticles with macropores. For example, Im et al. proposed a method to make hollow polymer particles with controllable holes on their surfaces [55]. Their research resulted in a protocol that generates pores on microparticles by evaporation of organic solvent from the inside microparticles. However, this method requires long time and to create pores on microparticle surface. In this work, to form pores and increase their size of original L100 particles, dichloromethane (T_b : 39.6°C) was used to swell the microparticles. With control of evaporation conditions, changes in the pore diameter were monitored with SEM analysis. Importantly, samples were incubated in an oven overnight, which is critical for the elimination of potential destabilization of drugs due to the presence of organic solvent. Without filtration, the size of microparticles was in the range of tens of micron to a sub-hundred micron (average diameter: 35 μm) (Figure 5).

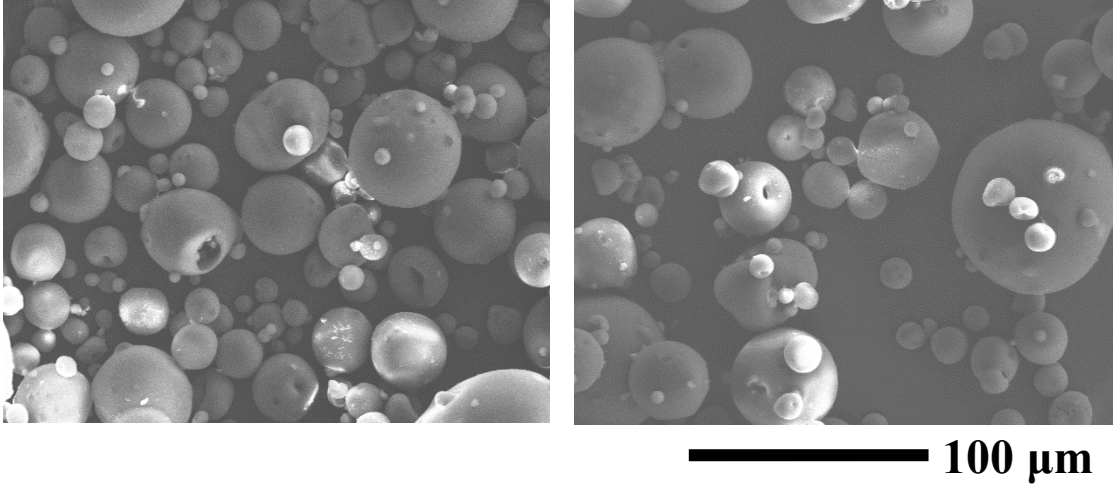


Figure 5 SEM images of 120 min sample

3.2 Effect of process parameters on pore formation and pore closure process

3.2.1 Effect of stirring and evaporation temperature on microparticles and pore closure process

To determine the effects of stirring and evaporation temperatures on pore formation and its size change, samples were prepared as described in section 2.2.1, and pore formation and size change were analyzed by SEM. In this work, we used ImageJ software to measure pore/particle size ratio and pored particle/total particle number ratio (see Figures 6 and 7 for analysis results). It was found that compared to L100-55 original polymer (control sample), all evaporation conditions induced the decrease in the population of small pored microparticles (0-5% and 5-10%), and increase in the population of large pored particles. A similar trend was observed for pored

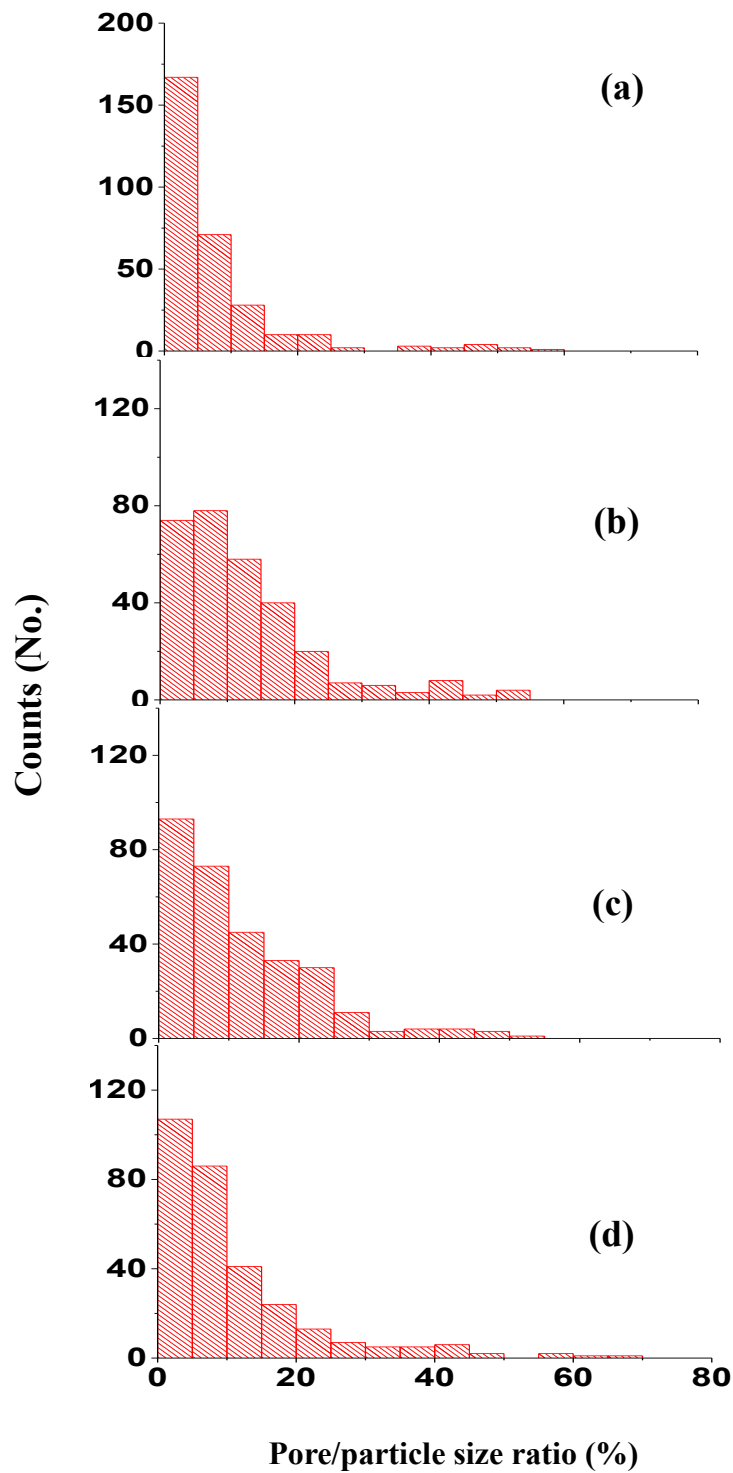


Figure 6 Histogram of sample pore/microparticles size ratio with sample fabrication conditions of a) original L100-55 polymer; b) evaporation at 65°C, then 37°C; c) 37°C overnight; and d) stirred at room temperature

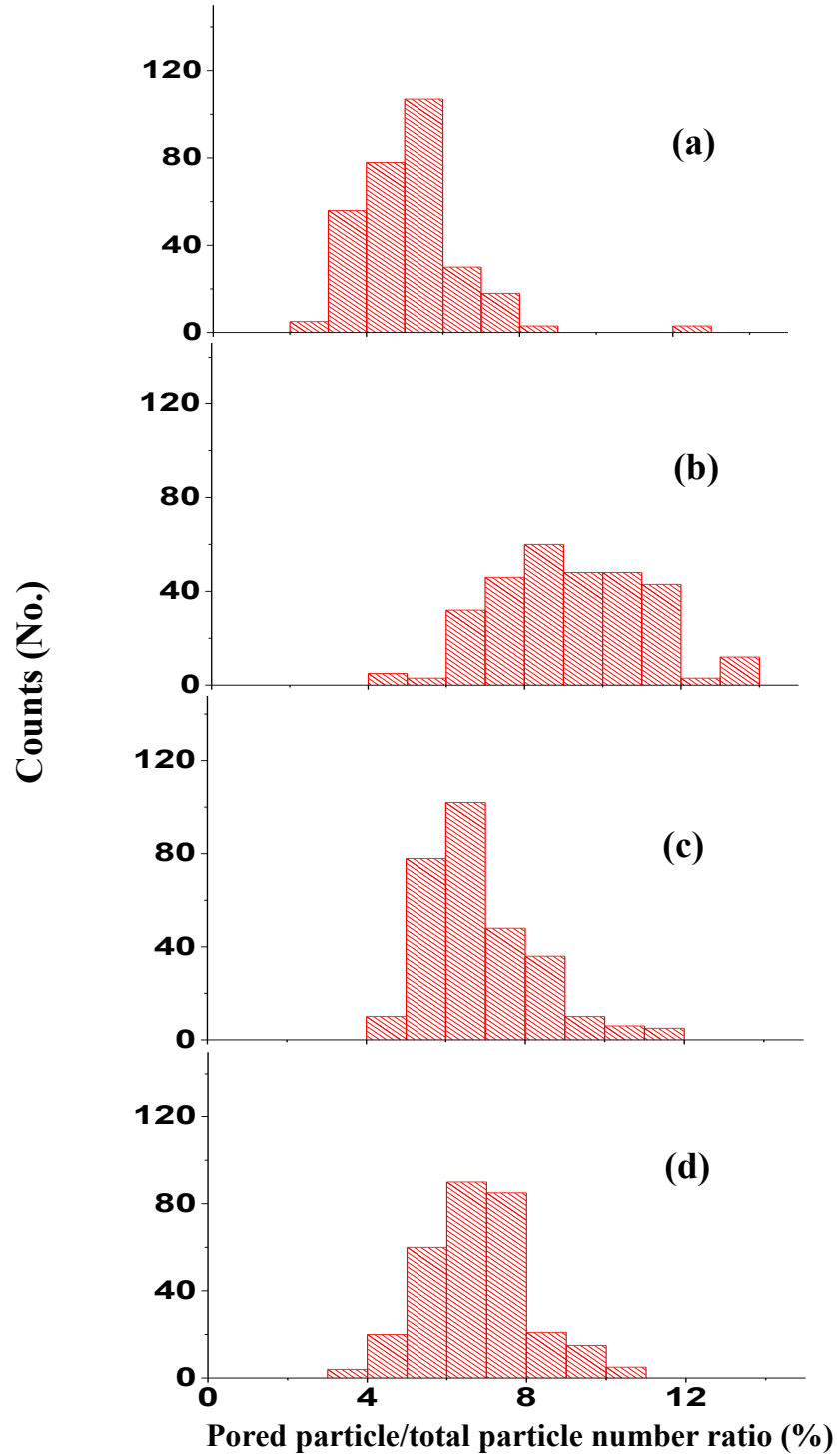


Figure 7 Histogram of pored microparticles/total microparticles number ratio with sample fabrications condition of a) original L100-55 polymer; b) evaporation at 65°C, then 37°C; c) 37°C overnight; and d) stirred at room temperature.

particle/total particle number ratio. Thus, it is concluded that polymer suspension in dichloromethane 1) after evaporation at 65°C, followed by 37°C incubation, 2) after evaporation at 37°C overnight, and 3) after stirring at room temperature resulted in the formation of pores and their size increase. It is also noted that steady evaporation for 30 min at 65°C followed by 37°C incubation overnight generated the most pored particles with the largest pore size among conditions tested in this work.

Our goal is to create microparticles with pH-sensitive pores for application to pH-sensitive biopharmaceuticals, which can maintain a pore closure at the acidic pH of the stomach to protect the pH-sensitive drug and open pores at an intestinal neutral pH to release the drug. Thus, a successful pore closure is a critical factor to our project. Furthermore, the pore closure method itself must be compatible with current pharmaceutical fabrication methods and biopharmaceuticals to preserve their bioactivity. To this end, we used a freeze-drying method (see section 2.2.2) to induce pore-closure of microparticles. SEM analysis was performed to compare the effect of different sample preparation methods on the size change of pores. Comparison of Figures 6 and 8 demonstrates the decrease of pore size due to freeze-drying process. In addition, freeze-drying resulted in decrease of the pored particle population (compare Figure 9 with Figure 7). Furthermore, no significant relationship between pore-formation methods and pore closure efficiency due to freeze-drying was observed in our experimental conditions. Incomplete pore closure of L100-55 polymer particles can be attributed to polydisperse size distribution and non-spherical morphology of the original microparticles.

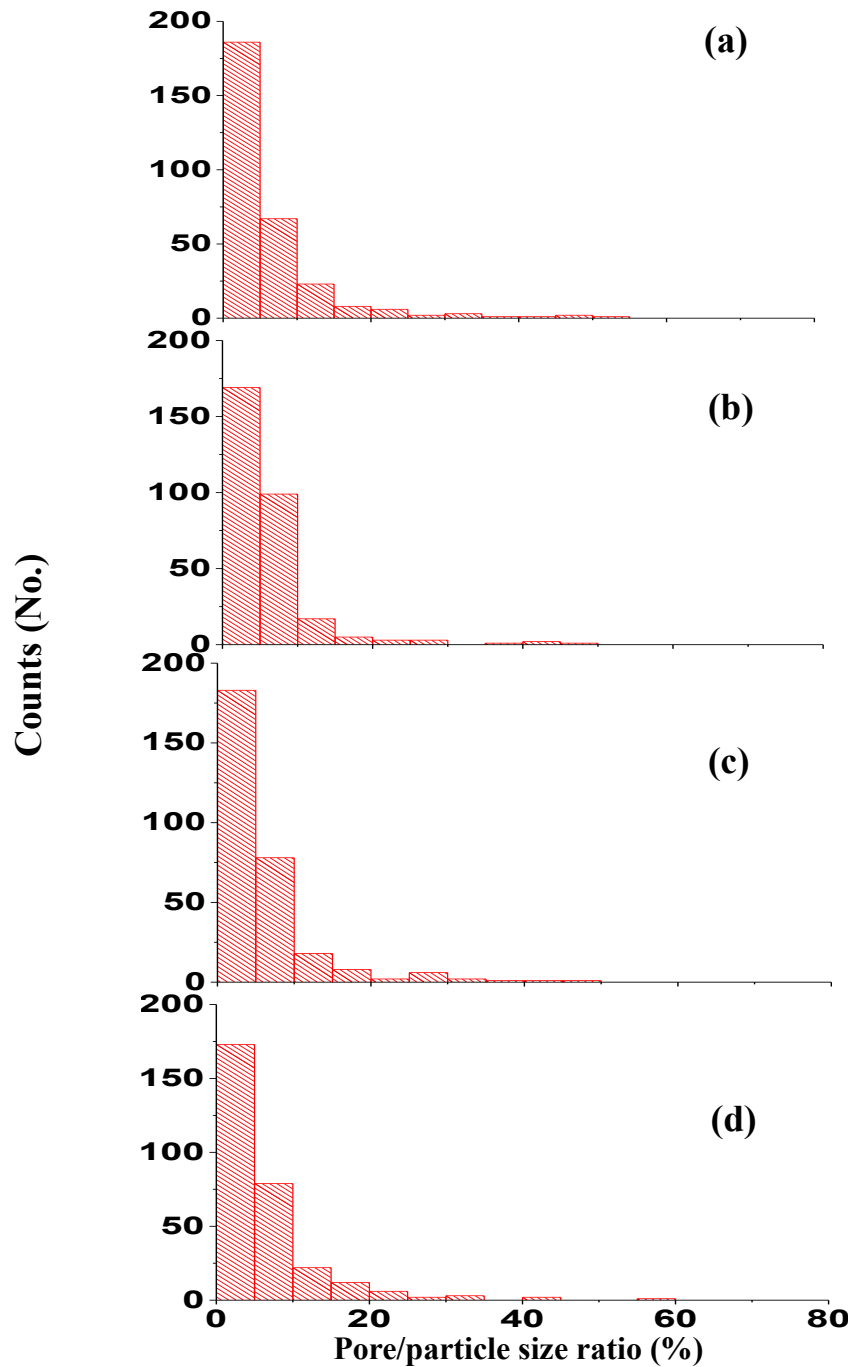


Figure 8 Histogram of pore/microparticles size ratio for freeze-dried with sample fabrication conditions of a) original L100-55 polymer; b) evaporation at 65°C, then 37°C; c) 37°C overnight; and d) stirred at room temperature

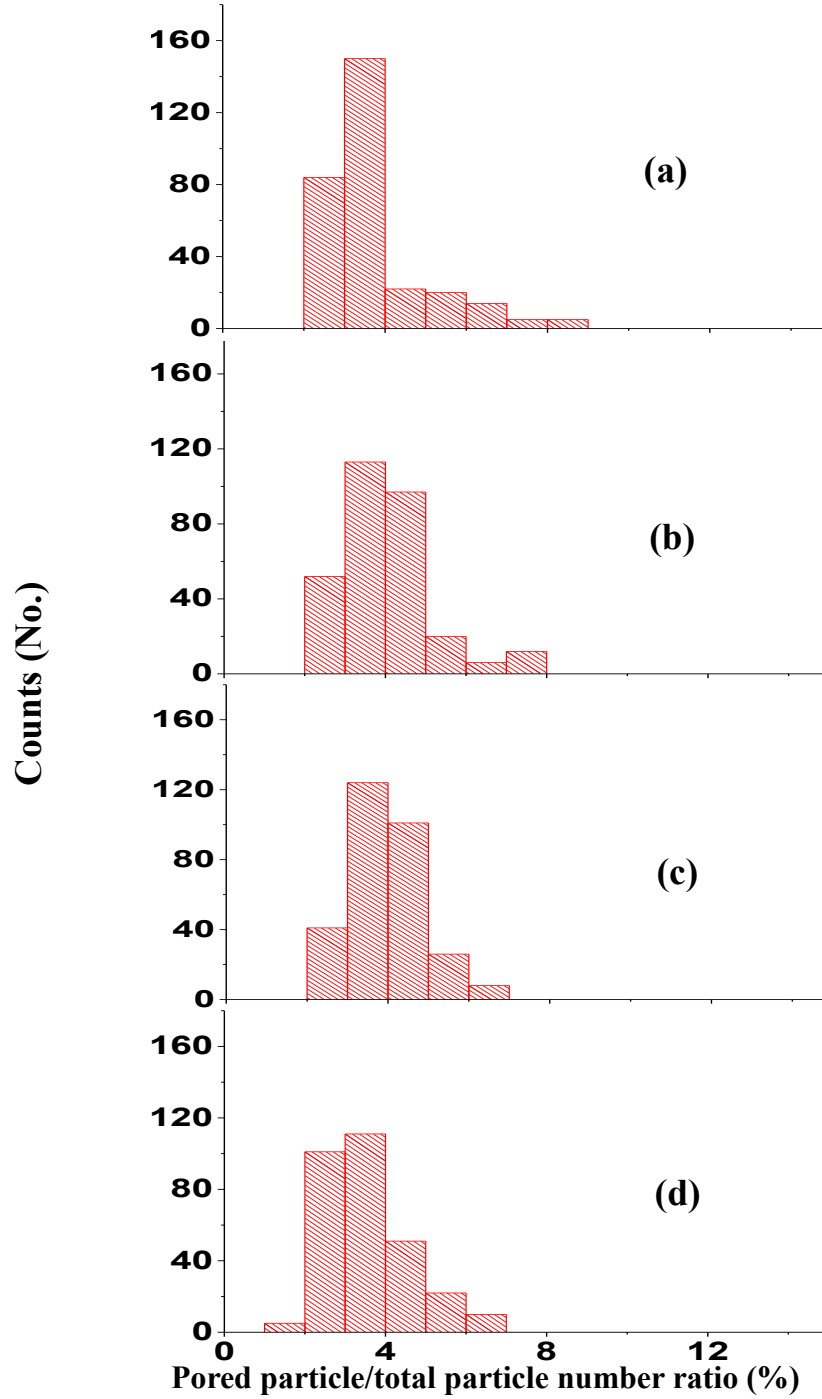


Figure 9 Histogram of pored microparticles/total microparticles number ratio for freeze-dried with fabrication conditions of a) original L100-55 polymer; b) evaporation at 65°C, then 37°C; c) 37°C overnight; and d) stirred at room temperature

3.2.2 Effect of rotary evaporation duration on microparticles and pore closure

The effects of rotary evaporation on the change in the size of pores were evaluated based on the hypothesis that solvent used to swell original polymer powders can further increase pore size during slow evaporation process. After the initial rotary evaporation, the microparticle samples were incubated at 65/37°C environment. This probably induce a burst evaporation of dichloromethane from microparticles, which may further increase the pore size on the microparticles' surface. For this purpose, samples were prepared at five different evaporation time (0 min, 15 min, 30 min, 60 min, and 120 min), and their pore/particle size ratio was characterized. As shown in Figure 10, it is evident that the pore size increases with the increase of evaporation time up to 60 min; however, no significant difference was observed between the 60 min and 120 min samples. Based on these results, 120 min sample was chosen for the encapsulation and release experiments.

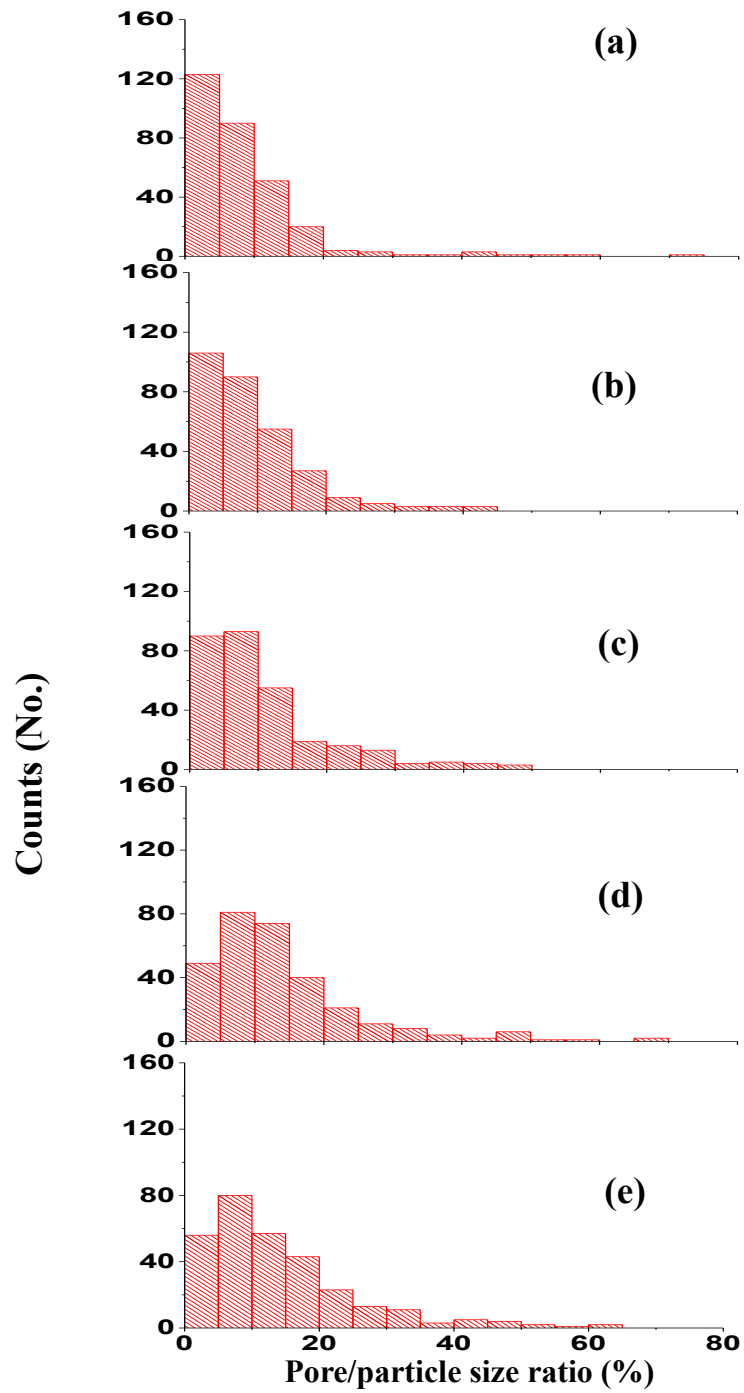


Figure 10 Histogram of pore/microparticles size ratio for microparticles prepared with rotated evaporation duration of a) 0 min; b) 15 min; c) 30 min; d) 60 min; or e) 120 min

3.3 FNPs encapsulation and visualization of release behavior

To examine the applicability of the fabricated pored microparticles in the simulated GI tract environment, 100 nm FNPs were encapsulated following the protocol described in the section 2.3.1. By employing fluorescence microscopy, pH-dependent release behavior of microparticles was monitored. As can be seen in Figure 11, in the simulated gastric environment, FNP-encapsulated microparticles maintained their intact spherical structure over the course of 2 hours of incubation. However, when the microparticles were subjected to simulated intestinal environment (pH 7.1), encapsulated FNPs were observed to be released from the microparticles (see Figure 12). By comparing the FNP release images for different time intervals to the control group (FNPs only, Figure 12 (i)), it can be seen that majority of 100 nm-sized FNPs leaked out after 20 min of incubation in pH 7.1. This can be explained by the rapid pore opening/dissolution behavior in the neutral pH environment, which is consistent with our hypothesis. Therefore, this study qualitatively illustrates that our pored microparticles system can encapsulate model drugs and protect them from gastric fluids, and then rapidly release them in the intestinal environment.

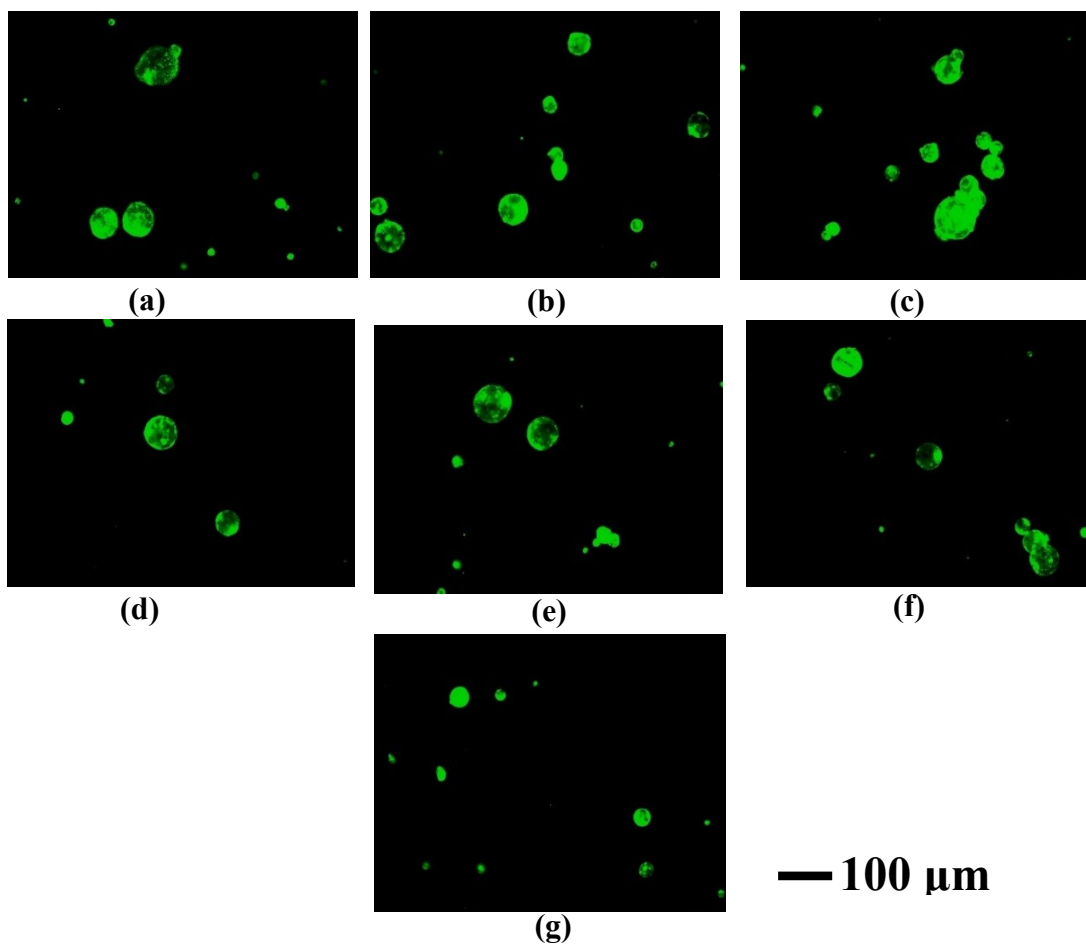


Figure 11 Fluorescence microscope images of FNP encapsulated microparticles in pH 2.0 buffer with incubation time a) 0 min; b) 10 min; c) 20 min; d) 30 min; e) 60 min; f) 90 min; or g) 120 min

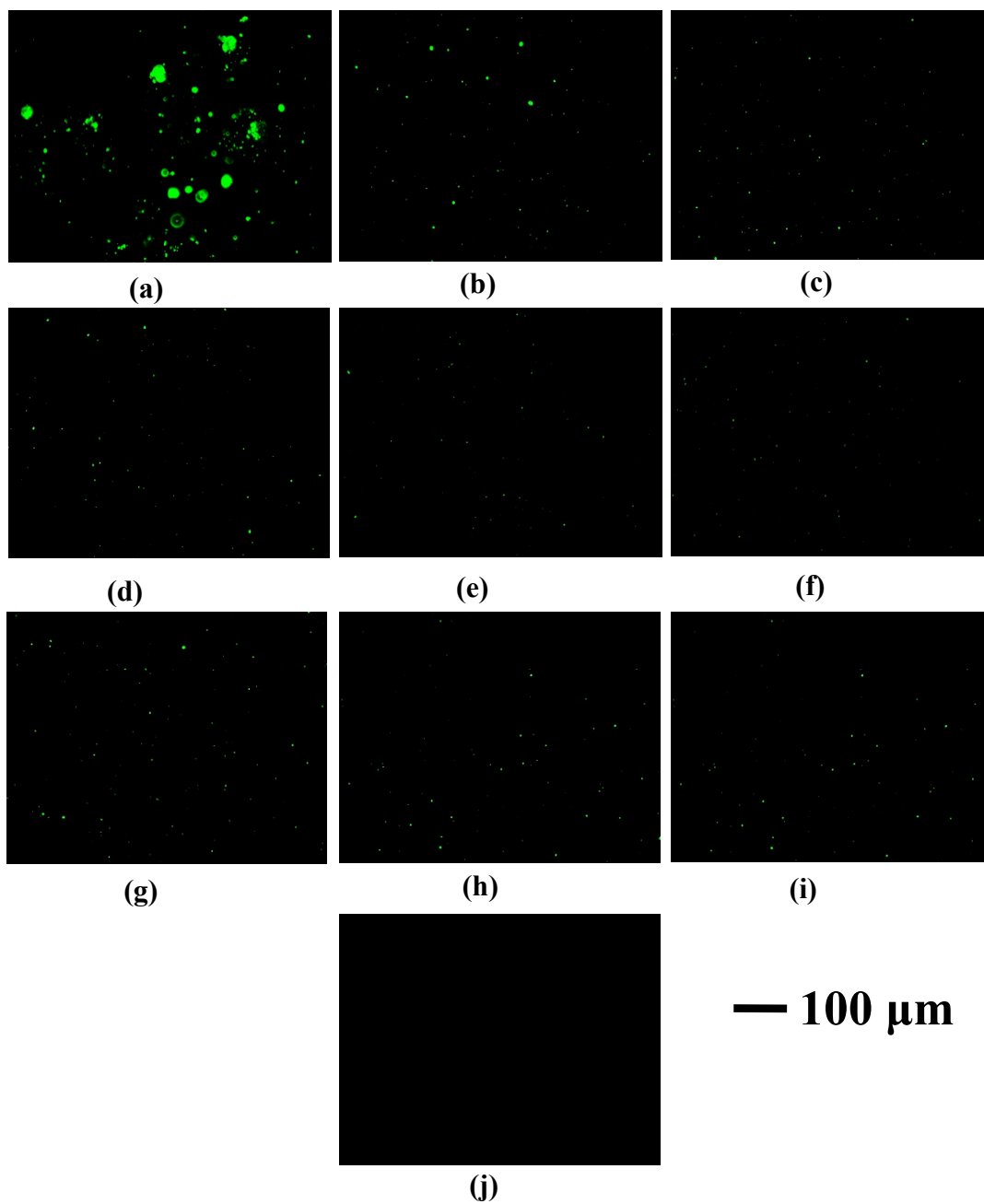


Figure 12 Fluorescence microscope images of FNP encapsulated microparticles in pH 7.1 buffer with incubation time a) 0 min; b) 10 min; c) 20 min; d) 30 min; e) 40 min; f) 50 min; g) 60 min; h) 240 min; i) 1000 times diluted FNPs stock solution in pH 7.1 buffer; and j) microparticles without FNP encapsulated

3.4 Encapsulation of Pravastatin and its release profile

After successful demonstration of the encapsulation and release behavior for FNPs, pravastatin was selected as the other encapsulant. Pravastatin sodium is a small molecule drug (MW=446.51 g/mol), which is reported to be water soluble and unstable in the gastric environment. Hence, microparticles' ability to prevent pravastatin from leaking out and preserving its bioactivity in the gastric environment, and releasing it in the intestinal environment will showcase the applicability of our microparticles drug delivery system.

3.4.1 Time-dependent pH responsiveness of pravastatin encapsulated microparticles by SEM imaging

To investigate the time dependent pH responsiveness of drug encapsulated microparticles and visualize the dissolution process of microparticles in the simulated GI environment, SEM analysis for samples with different time intervals was performed. It should be noted that samples were shaken at 37°C during the entire 6 hours of incubation (2 hours in gastric pH and 4 hours in intestinal pH) to mimic the physiological digestion process. At each time point, samples were taken from the mixture under incubation. Microparticles in the acidic environment maintained their spherical morphology for the entire 2 hours of incubation as can be seen from Figure 13. After transferring the samples to pH 7.1, the particles started to change their shapes

and dissolved immediately (see Figure 14). After 30 min of incubation in pH 7.1, the dissolution of microparticles leading to several fragments can clearly be observed. It should be noted that this release behavior matches with the FNP- encapsulated fluorescent microscopy results.

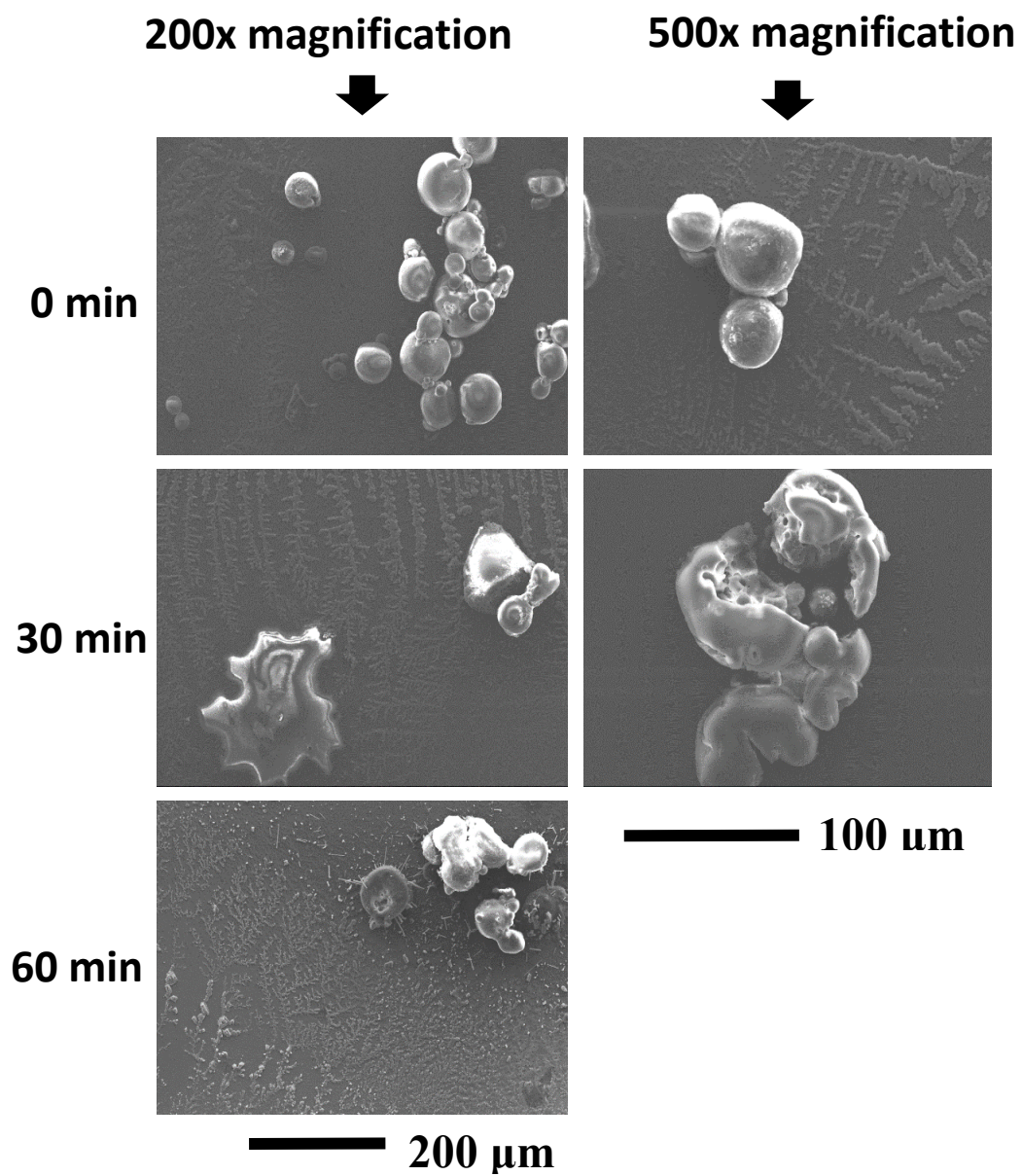


Figure 14 SEM images of pravastatin sodium encapsulated microparticles in pH 7.1 buffer

3.4.2 Pravastatin release profile

SEM analysis provided us with the visual confirmation that microparticles dissolved in the intestinal environment to release the encapsulated pravastatin. To qualitatively confirm these findings, a HPLC-MS method was employed. As Figure 15 shows, the peaks of pravastatin sodium ($M[\text{PRA-Na}] = 447.4$) and pravastatin potassium ($M[\text{PRA-K}] = 463.4$) were observed in the spectrum at 6.0-6.3 min retention time. The existence of pravastatin potassium is due to the presence of KCl salt in pH 2.0 buffer. Also, it needs to be noted that there are also two other higher intensity peaks in the lower mass of the spectrum, which correspond to potassium phosphate and sodium phosphate. As such, phosphate salt was used to prepare pH 7.1 buffer. Thus, all the major peaks in the MS spectrum can be easily assigned. According to the list of pravastatin and its metabolite in the introduction, the mass spectroscopy result confirmed that the peak of mass was identical to that of pravastatin; however, it can be either pravastatin sodium, its isomer α -pravastatin sodium, or a mixture of the two. Consequently, a separate detection and analysis was performed using HPLC-UV.

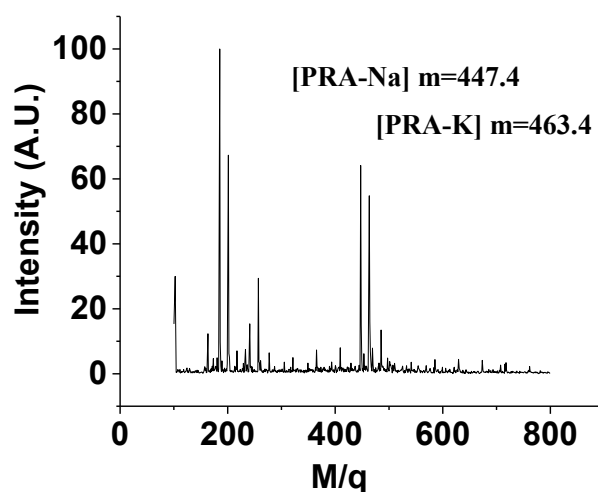


Figure 15 HPLC-MS spectrum of pravastatin encapsulated microparticles after 6 hours incubation in simulated GI tract pH

HPLC-UV method was used to determine the presence of pravastatin sodium in the released sample and to quantify the pravastatin sodium encapsulated microparticles release behavior. First, the stability of pravastatin at room temperature was tested. One-day storage of a 20 $\mu\text{g/mL}$ pravastatin sodium solutions in pH 7.1 buffer did not show any significant difference in HPLC-UV signal after storage. Figure 16 shows the observed retention time was 2.8-3.1 min under the HPLC-UV condition as described in section 2.5.4. This supports the absence of pravastatin degradation during the HPLC-UV test. After being treated with pH 2.0 buffer for 15 min, a significant peak reduction occurred at 2.8-3.1 min, while the 3` α -pravastatin peak was newly observed at the retention time of 3.3-3.7 min, as shown in Figure 17. The difference of peak provided a way to quantitatively analyze the pravastatin without the interference of its 3` α isoform.

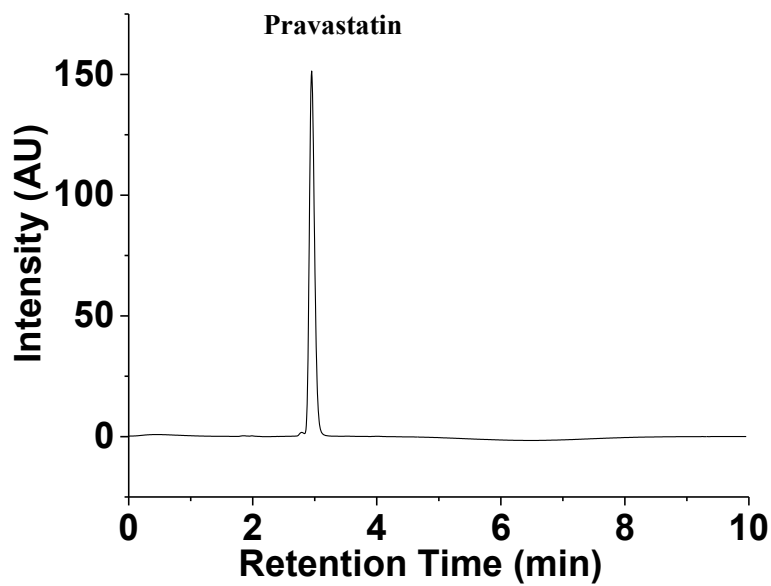


Figure 16 HPLC-UV spectrum of 20 µg/mL pravastatin sodium in pH 7.1 buffer at 0 min

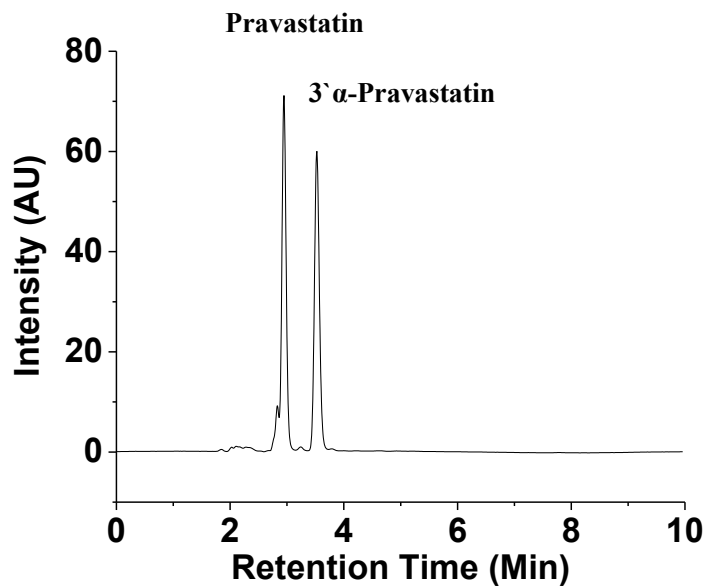


Figure 17 HPLC-UV spectrum of 20 µg/mL pravastatin sodium incubated at 37°C and pH 2.0 environment for 15 min

To calculate the concentration of pravastatin in the released sample, pravastatin sodium with two different concentrations in pH 7.1 buffer were tested: 1) 10-50 $\mu\text{g/mL}$ with the step size of 10 $\mu\text{g/mL}$ and 2) 2-10 $\mu\text{g/mL}$ with the step size of 2 $\mu\text{g/mL}$. The calibration curve for each condition is shown in Figure 18 and 19, respectively. The pravastatin sodium concentration and HPLC-UV peak integral showed a good linear relationship, with $R=0.9999$ for 10-50 $\mu\text{g/mL}$ and $R=0.9996$ for 2-10 $\mu\text{g/mL}$.

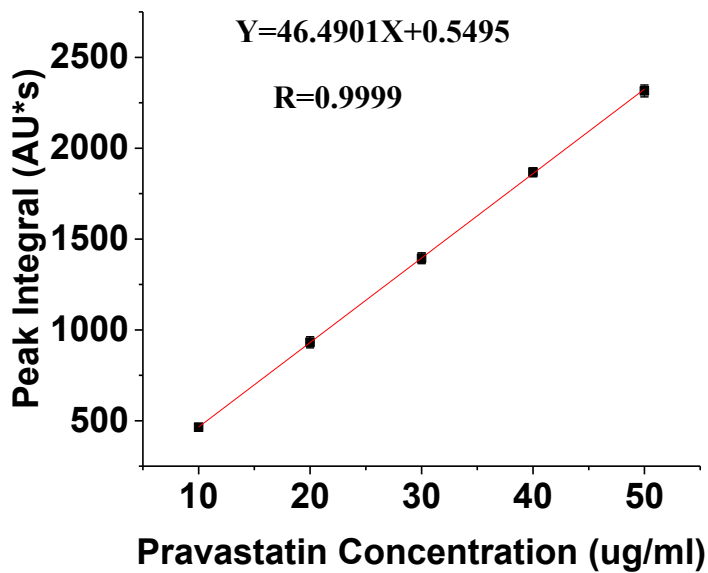


Figure 18 HPLC-UV calibration curve of Pravastatin sodium in pH 7.1 buffer with concentration ranging from 10-50 $\mu\text{g/mL}$ and step size of 10 $\mu\text{g/mL}$

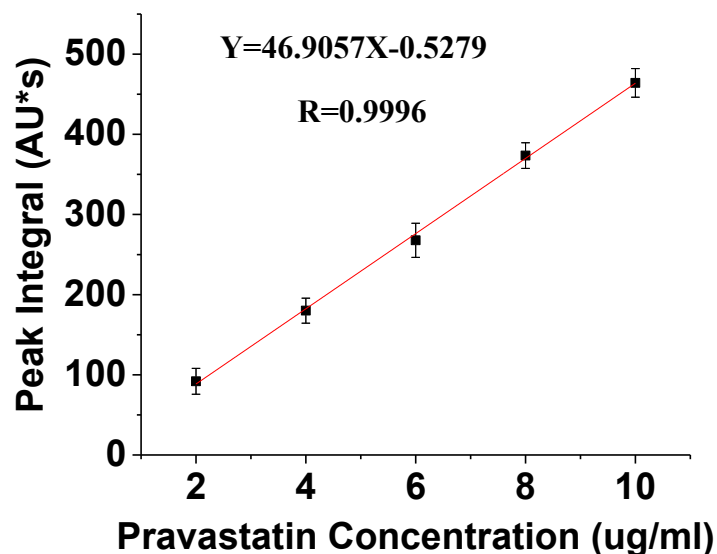


Figure 19 HPLC-UV calibration curve of Pravastatin sodium in pH 7.1 buffer with concentration ranging from 2-10 $\mu\text{g/mL}$ and step size of 2 $\mu\text{g/mL}$

After the acquisition of the pravastatin calibration curve, the release of pravastatin sodium encapsulated microparticles was investigated. Apart from the sample group, pravastatin encapsulated microparticles with the same concentration was treated with pH 7.1 directly under intense shaking for 6 hours as a control group. According to the SEM analysis and fluorescence microscopy results, the microparticles should be completely dissolved after 4 hours of pH 7.1 treatment. Since pravastatin has been proven to be stable at pH 7.1 for at least one day, the control group should represent the total pravastatin encapsulated in the microparticles. Figure 20 and the calibration curve of Figure 18 have shown that in the experimental conditions, pravastatin concentration of the control group is 25.83 $\mu\text{g/mL}$. The total volume of released fluid was 18 mL (4 mL acidic buffer and 14 mL basic buffer), while the initial polymer

added for each release test was 40 mg. Thus, the loading capacity (LC%) can be calculated by the formula as shown below.

$$LC\% = \frac{[\text{Entrapped Drug}]}{\text{Microparticles weight}} \times 100 = \frac{25.83\mu\text{g}/\text{ml} \times 18\text{ml}}{40\text{mg}} = 1.16\%$$

To get a better picture of time-dependent pH response, the pravastatin release curve in the GI tract environment was also acquired. As Figure 21 shows, 2-hour incubation at acidic pH did not exhibit any significant change in the concentration of pravastatin. The pravastatin concentration ranged from 2.14-4.28 $\mu\text{g}/\text{mL}$, which was 8.3-16.6% of the total encapsulated pravastatin sodium. The observation of small pravastatin concentration can be explained by two reasons: 1) two washing steps removed most of the pravastatin sodium outside of microparticles; however, there might still be a minor amount of pravastatin sodium left attached outside of the microparticles' wall; 2) pravastatin leakage occurred from the microparticles with irregular morphology, whose pores cannot be closed properly. Furthermore, an initial increase of pravastatin concentration followed by a slowly decrease over time during acidic incubation perfectly matches our prediction that after the release of pravastatin from the microparticles whose pores are not completely sealed, the drug started to degrade in the gastric pH and lost its bioactivity.

Exposure to pH 7.1 induced a significant level of pravastatin release, i.e. $\sim 55\%$ of the total encapsulated pravastatin, compared to the acidic phase. Then the pravastatin concentration reached saturation in the release profile at around 61% in 1 hour time

interval. After that, the pravastatin concentration remained the same until the end of the whole process. Also, after 6 hours of incubation, the sample was vortexed continuously for 20 min to ensure complete release of pravastatin from the microparticles. However, no significant difference was observed compared to 1 hour sample, indicating that microparticles were completely dissolved within 1 hour of exposure to pH 7.1 buffer. This result shows that around 61% of the pravastatin was preserved after being incubated in a GI tract environment.

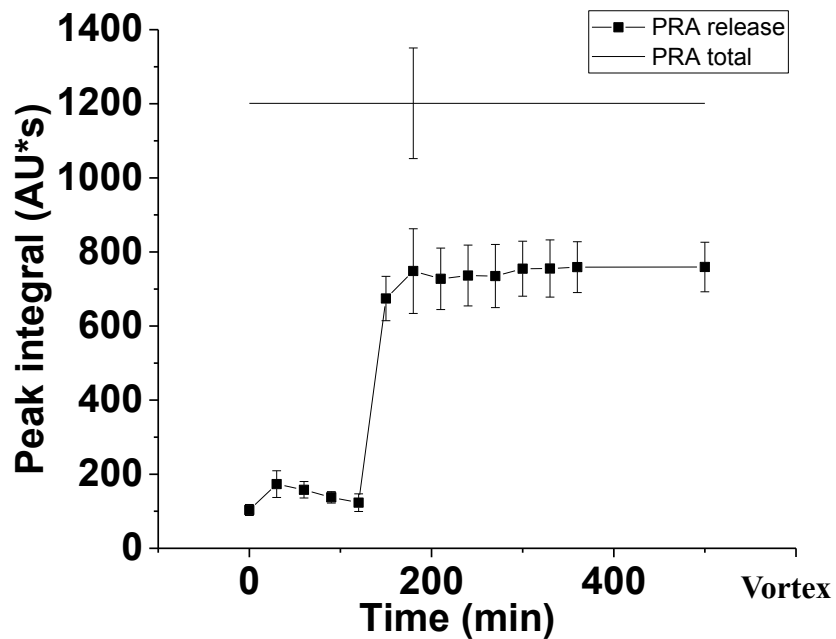


Figure 20 HPLC-UV peak integral of pravastatin sodium encapsulated microparticles in response of incubation time in GI tract pH, (PRA total: the peak integral of pravastatin sodium encapsulated microparticles with pH 7.1 applied from the start of incubation follo

In parallel, the same concentration of pravastatin as one encapsulated into microparticles was exposed to simulated GI tract pH condition. Without using microparticles, the pravastatin concentration significantly dropped when placed in pH 2.0 buffer. Within 30 min of incubation in the acidic environment, 74% of pravastatin degraded. Then the value slowly reached to a stationary point after 1 hour incubation in pH 2.0 buffer, where 84% of the pravastatin degraded. Thus, only 16% of remaining stability was preserved without using our microparticles.

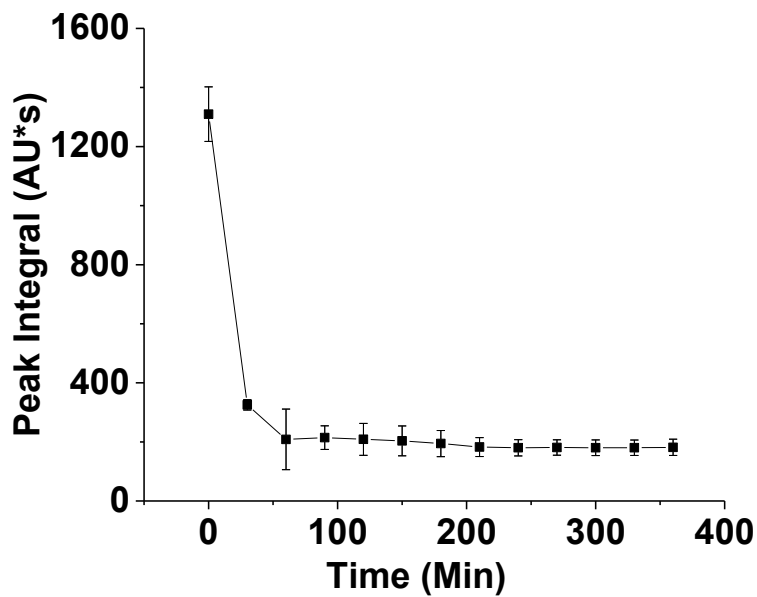


Figure 21 HPLC-UV peak integral of pravastatin sodium incubated in simulated GI tract pH without microparticles, as the control group

The results of the release test and control group show that our pored microparticles are capable of protecting pravastatin from harsh GI tract pH conditions (16% to 61% preserved). Our pored microparticles are favorable for environment-sensitive drugs, because it does not involve the drug during sample preparation compared to other microencapsulation methods such as emulsion and spray-drying. Additionally, at the encapsulation stage, the drug solution supernatant after centrifugation can always be collected and recycled for the next batch of encapsulation. Therefore, pored L100-55 microparticles-based drug delivery system represents a cost-effective and viable method for various environment-sensitive drugs.

3.5 Pore formation mechanism exploration

A ^1H NMR test was performed to determine the pore formation mechanism of L100-55 polymer-based microparticles in dichloromethane. First, the ^1H NMR spectrum of original polymer was acquired as the control group (see Figure 22).

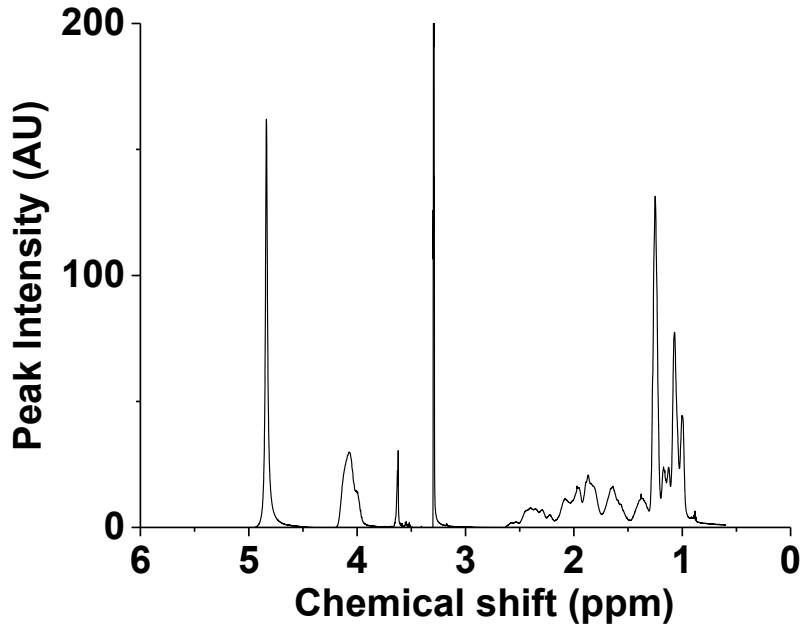


Figure 22 ^1H NMR spectrum of the L100-55 polymer in CD_3OD

The acquired ^1H NMR spectrum has an overlapped multiplet at $\delta=1.0$, a singlet at $\delta=1.2$, a sharp singlet at $\delta=3.3$ (CD_3OD) and a singlet at $\delta=3.6$, a broad singlet at $\delta=4.0$ and a singlet at $\delta=4.9$.

The ^1H NMR spectrum of DCM supernatant after the sample preparation (see Figure 23) shows a significant difference in peak locations compared to the original L100-55 polymer. The main reason is the existence of ~ 2.3 wt% Polysorbate 80, a commonly used surfactant in microparticles fabrication. Figure 24 shows the structure of Polysorbate 80. Its ^1H NMR is given in the literature (see Table 3.1), matching the ^1H NMR spectrum obtained from our sample [56].

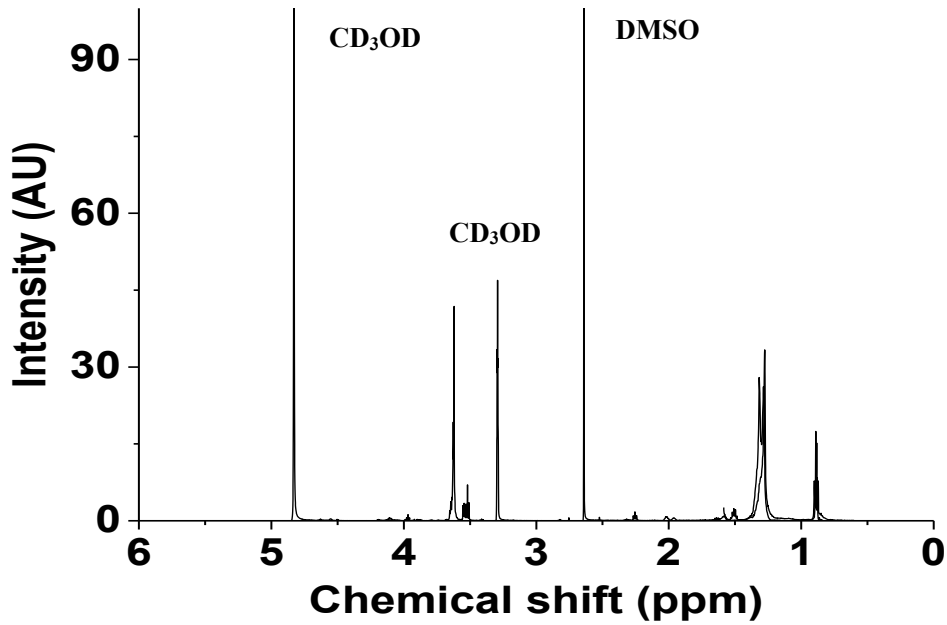


Figure 23 ^1H NMR spectrum of DCM supernatant of 0 min rotated evaporation sample in CD_3OD with 10mM DMSO as a reference

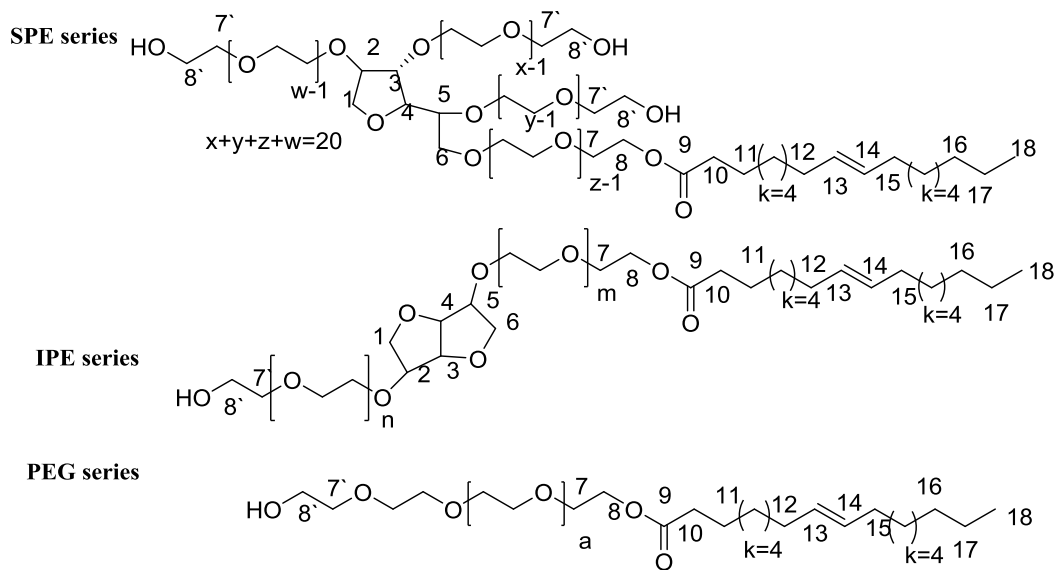


Figure 24 Schematic representation of Polysorbate 80 chemical structure and ^1H NMR proton positions

After acquisition of ^1H NMR of the DCM supernatant for microparticles prepared under different time interval conditions, the major peaks were assigned, and the intensity of those peaks was indicated according to DMSO reference. The results are shown in Table 3.1.

Table 3.1 ^1H NMR results summary of polymer dissolution test by rotation time

^1H position No.	Peak shape	Chemical shift δ	Peak intensity (AU) of Samples (min)				
			0	15	30	60	120
7, 8`	multiplet	~ 3.70	120	432	448	471	479
CH_2 (k)	Broad doublet	1.34	308	609	610	607	599
18	triplet	~ 0.90	53	98	95	89	87

The trend in the table shows that dissolution of Polysorbate 80 in dichloromethane rapidly occurs from 0 min to 15 min rotary evaporation and becomes stable from 15 min to 120 min. To determine if there are chemical groups of Polysorbate 80 attached to our polymer and involved in pore formation and further to determine the relationship between this ^1H NMR observation and pore formation, Polysorbate 80 was treated with the same 120 min rotary evaporation process. Then ^1H NMR samples were prepared with original Polysorbate 80 as a control. The comparison of ^1H -NMR major signals between the Polysorbate 80-120 min sample, Polysorbate 80-original polymer, and 120 min sample are summarized in Table 3.2.

Table 3.2 ¹H NMR results summary of Polysorbate 80 dissolution test compared to 120 min sample

¹ H position No.	Peak shape	Chemical shift δ	Peak intensity (AU) of Samples		
			Polysorbate 80 original	Polysorbate 80 120min	120min sample
7, 8'	multiplet	~3.70	4516	3045	479
7'	triplet	3.6	278	184	65
CH ₂ (k)	Broad doublet	1.34	1478	988	599
12,15	doublet	2.06	226.87	153	N/A
18	sharp triplet	0.9	205.02	139	87

After the rotary evaporation of Polysorbate 80 in dichloromethane, the ¹H NMR showed no difference in each major peak, indicating that no chemical composition change occurred to Polysorbate 80. However, ¹H NMR signal ratios (other peaks/proton 18 intensity, proton 18 signal as a reference) of position 7, 7' and 8 protons are much smaller for the 120 min sample, compared to that of other two conditions, indicating that chemical groups related to -O-CH₂-CH₂-O- might detach from Polysorbate 80 during the rotary evaporation and were involved in pore formation. To further confirm this result, Polysorbate 80 and PAA-co-PMMA polymer were mixed, mimicking the same ratio of our pH-responsive polymer, following the same 120 min sample preparation procedure. Then the ¹H NMR spectra were acquired as summarized in Table 3.3.

Table 3.3 ¹H NMR results summary of PAA-*co*-PMMA and Tween dissolution test

¹ H position No.	Peak shape	Chemical shift δ	Peak intensity (AU)	
			Trial 1	Trial 2
7, 8'	multiplet	~3.70	3498	2293
CH ₂ (k)	Broad doublet	1.34	1055	741
18	sharp triplet	0.9	159	115

Comparison of the results in Table 3.2 and Table 3.3 shows no significant difference in the peak ratios between PAA-*co*-PMMA with Polysorbate 80 and Polysorbate 80 only. These results indicate that there is no chemical composition change in either Polysorbate 80 or our polymer during the rotated evaporation process. The peak difference shown in Table 3.2 after sample preparation may be induced by the presence of 0.7 wt% sodium lauryl sulfate (Figure 25) in the commercial form of our original polymer. In the literature, in CD₃OD, sodium lauryl sulfate has three major ¹H NMR signals, $\delta=3.7$, $\delta=1.35$., and $\delta\sim 0.9$, which overlap with most of the major ¹H NMR signals of Polysorbate 80 [56]. Thus, the mixed signal of these components may result in the peak ratio change observed in this experiment.

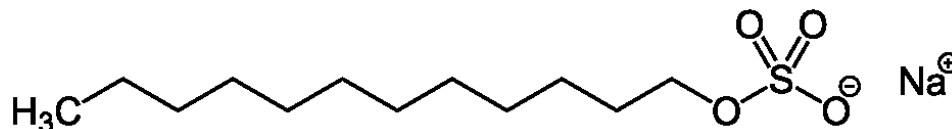


Figure 25 Chemical structure of sodium lauryl sulfate [57]

4 Conclusion and Future Work

In our efforts to develop an ‘emulsion-free’ oral delivery system for pH-sensitive macromolecular drugs, the capability of pH-responsive pored microparticles was investigated. The microparticles were designed to overcome the technical challenges of the current microparticles-based drug delivery systems, including the exposure of drugs to organic solvents during particle fabrication stage, loss of bioactivity in GI tract, and low yield. In a systematic approach, Eudragit L100-55 microparticles with pH responsive pores were generated by a novel solvent evaporation method. After successful fabrication of pored microparticles, the pore size controllability was tested and optimized by varying the process parameters, such as the steady evaporation temperature, stirring, and rotated solvent evaporation duration. These experiments provided us with valuable insights that the factors related to solvent evaporation rate and degree of solvent swelling of polymers had a direct effect on pore formation (pore/particle size ratio and pored particles/total particles number ratio). A novel technique to close the pores of microparticles by freeze-drying was employed, and proven to be effective through SEM analysis. Extent of pore closure is critical to ensure the efficacy of drugs against the harsh environment of the stomach. The two model drugs, FNPs and pravastatin sodium, were encapsulated using a unique technique that utilizes vacuum cycles for drug loading. The successfulness of encapsulation and pH responsiveness of the delivery system in a time-dependent simulated GI tract

environment was demonstrated by fluorescence microscopy and SEM imaging. The pores remained intact (closed), and the microparticles were capable of preventing model drugs from leaking out in a pH 2.0 environment (gastric pH) while preserving their bioactivity, and then burst releasing most of the encapsulated drugs within 30 min after exposure to a neutral pH (intestinal pH). By quantifying the release behavior of pravastatin, it was found that 61% of the encapsulated drug was successfully preserved in the gastric pH, and later released less than 30 mins (the first measurement time point) after exposure to a neutral pH environment. In absence of our pored microparticles system, pravastatin activity dropped to a significantly low level (16%). Thus, the high preservation efficiency, efficient release profile of drugs from pored microparticles, and precise control of pore opening in response to pH change were proved to be the key factors that successfully implemented our proof-of-concept pored microparticle drug delivery system. Although our work has not been applied to *in vivo* demonstration of the concept, findings from this work clearly illustrate the potential of our smart drug delivery system. Importantly, the pores on the microparticles were observed to be up to a few microns in diameter. Therefore, it is believed that not only small molecule drugs such as pravastatin, but also many large molecule drugs that have complicated structures, for example proteins, can also be encapsulated into our microparticles. Also, through a preliminary exploration of a pore formation mechanism utilizing ^1H NMR, it was determined that the pore formation did not induce any chemical composition change of the polymer. However, further research still needs to be done to completely understand the principle behind it.

In future work, microparticles preparation procedure will be further optimized to increase the pore size and population of the pored particles. The appropriate size of microparticles will be selected for more favorable intestinal absorption. To better understand the concept behind pore formation, more experiments will be designed to identify the pore formation mechanism. Lastly, to further confirm the bioactivity of released drug, *in vivo* studies need to be carried out to corroborate the *in vitro* findings.

References

1. Jain, K. K. Drug delivery system. Second edition.
2. Jain KK (2014) Transdermal drug delivery: technologies, markets and companies. *Jain PharmaBiotech Publications*, Basel, pp 1–280
3. Ranade, V. V, & Cannon, J. B. (2011). Drug delivery systems. 3rd ed. Boca Raton: CRC Press.
4. Wang, B., Hu, L., & Siahaan, T. Drug delivery : principles and applications. Second edition. .
5. Muhammad, Z., Junaid, Q., Hira, E., Rai Muhammad, S., Hafeez ullah, K., Fazal Rehman, S., & Muhammad Shafiq ur, R. (2016). Oral controlled release drug delivery system and Characterization of oral tablets; A review. *Pakistan Journal Of Pharmaceutical Research*, Vol 2, Iss 1, Pp 67-76 (2016), (1), 67.
6. Belyakov IM, Ahlers JD. What role does the route of immunization play in the generation of protective immunity against mucosal pathogens? *J. Immunol.* 183, 6883–6892 (2009).
7. Holmgren J, Svennerholm AM. Vaccines against mucosal infections. *Curr. Opin. Immunol.* 24, 343–353 (2012).
8. Nudel I, Elnekave M, Furmanov K et al. Dendritic cells in distinct oral mucosal tissues engage different mechanisms to prime CD8+ T cells. *J. Immunol.* 186, 891–900 (2011).
9. Lesterhuis WJ, de Vries IJ, Schreiber G et al. Route of administration modulates the induction of dendritic cell vaccine-induced antigenspecific T cells in advanced melanoma patients. *Clin. Cancer Res.* 17, 5725–5735 (2011).
10. Durando P, Iudici R, Alicino C et al. Adjuvants and alternative routes of administration towards the development of the ideal influenza vaccine. *Hum. Vaccin.* 7 (Suppl.), S29 – S40 (2011) .
11. Ranade, V. V., & Cannon, J. B. (2011). Oral Drug Delivery. *Drug Delivery Systems*, 169–242.

12. Owen, R. L., Apple, R. T. & Bhalla, D. K. (1986). Morphometric and cytochemical analysis of lysosomes in rat Peyer's patch follicle epithelium: their reduction in volume fraction and acid phosphatase content in M cells compared to adjacent enterocytes. *Anat. Rec.* 216, 521–7. Yang, M., & Frokjaer, S. (2009). Novel Formulation Approaches for Peptide and Protein Injectables. *Delivery Technologies for Biopharmaceuticals: Peptides, Proteins, Nucleic Acids and Vaccines*, 9–28.
13. Bernkop-Schnürch, A. (2009). *Oral delivery of macromolecular drugs: barriers, strategies and future trends*. Dordrecht: Springer.
14. Ganta, S., Deshpande, D., Korde, A., & Amiji, M. (2010). A review of multifunctional nanoemulsion systems to overcome oral and CNS drug delivery barriers. *Molecular Membrane Biology*, 27(7), 260-273. doi:10.3109/09687688.2010.497971
15. Bourganis, V., Karamanidou, T., Kammona, O., & Kiparissides, C. (2017). Polyelectrolyte complexes as prospective carriers for the oral delivery of protein therapeutics. *European Journal Of Pharmaceutics & Biopharmaceutics*, 11144-60. doi:10.1016/j.ejpb.2016.11.005
16. Roberts, M. J., Bentley, M. D., & Harris, J. M. (2002). Chemistry for peptides and protein PEGylation. *Adv. Drug Deliv. Rev.*, 54, 459–476.
17. Elliott, S., Lorenzini, T., Asher, S. *et al.* (2003). Enhancement of therapeutic protein *in vivo* activities through glycoengineering. *Nat. Biotechnol.*, 21, 414–421.
18. Havelund, S., Plum, A., Ribel, U. *et al.* (2004). The mechanism of protraction of insulin detemir, a long-acting, acylated analog of human insulin. *Pharm. Res.*, 21, 1498–1504.
19. Alonso, M. J., Gupta, R. K., Min, C., Siber, G. R., & Langer, R. (1994). Biodegradable microspheres as controlled-release tetanus toxoid delivery systems. *Vaccine*, 12(4), 299–306.
20. Raghuvanshi, R. S., Katare, Y. K., Lalwani, K., Ali, M. M., Singh, O., & Panda, A. K. (2002). Improved immune response from biodegradable polymer particles entrapping tetanus toxoid by use of different immunization protocol and adjuvants. *International Journal Of Pharmaceutics*, 245(1-2), 109–121.
21. Slobbe, L., Medlicott, N., Lockhart, E., Davies, N., Tucker, I., Razzak, M., & Buchan, G. (2003). A prolonged immune response to antigen delivered in poly (ϵ -caprolactone) microparticles. *Immunology & Cell Biology*, 81(3), 185–191. doi:10.1046/j.1440-1711.2003.01155.x

22. Fernandez-Urrusuno, R., Calvo, P., Remuñan-López, C., Vila-Jato, J. L., & Alonzo, M. J. (1999). Enhancement of Nasal Absorption of Insulin Using Chitosan Nanoparticles. *Pharmaceutical Research*, 16(10), 1576-1581.
23. Nagavarma, B. V. N., Yadav, H. K., Ayaz, A., Vasudha, L. S., & Shivakumar, H. G. (2012). Different techniques for preparation of polymeric nanoparticles—a review. *Asian J. Pharm. Clin. Res*, 5(3), 16-23.
24. Nihant, N., Stassen, S., Grandfils, C., Jerome, R., & Teyssie, P. (1994). Microencapsulation by coacervation of PLGA: III. Characterization of the final microspheres. *Polym. Int.* 34: 289–299.
25. Uchida, T., Yagi, A., Y. Oda, & S. Goto. (1996). Microencapsulation of ovalbumin in poly (lactide-co-glycolide) by an oil-in-oil (o/o) solvent evaporation method. *J. Microencapsulation*. 13: 509–518.
26. Cózar-Bernal, M. J., Holgado, M. a, Arias, J. L., Muñoz-Rubio, I., Martín-Banderas, L., Alvarez-Fuentes, J., & Fernández-Arévalo, M. (2011). Insulin-loaded PLGA microparticles: flow focusing versus double emulsion/solvent evaporation. *Journal of Microencapsulation*, 28(5), 430–441.
27. Reis, C. P., Neufeld, R. J., Vilela, S., Ribeiro, A. J., & Veiga, F. (2006). Review and current status of emulsion/dispersion technology using an internal gelation process for the design of alginate particles. *Journal of Microencapsulation*, 23(3), 245–257.
28. Nihant, N., S. Stassen, C. Grandfils, R. Jerome, and P. Teyssie (1994) Microencapsulation by coacervation of PLGA: III. Characterization of the final microspheres. *Polymer. Int.* 34: 289-299.
29. Kas, H. S. and L. Oner (2000) Microencapsulation using coacervation. pp. 301-328. In: D. L. Wise (ed.). *Handbook of Pharmaceutical Controlled Release Technology*. Marcel Dekker, Inc., New York, USA.
30. Burgess, D. J. and A. J. Hickey (1994) Microsphere technology and applications. pp. 1-29. In: J. Swarbrick and J. C. Boylan (eds.). *Encyclopedia of Pharmaceutical Technology*. Marcel Dekker, Inc., New York, USA.
31. Wu, W. S. (1995) Preparation, characterization, and drug delivery applications of microspheres based on biodegradable lactic/glycolic acid polymers. pp. 1151-1200. In: D. L. Wise (ed.). *Encyclopedic Handbook of Biomaterials and Bioengineering*. Marcel Dekker, New York, USA.
32. Ryu, K., & Dordick, J. S. (1992). How do organic solvents affect peroxidase structure and function?. *Biochemistry*, 31(9), 2588-2598.

33. Raghuvanshi, R. S., Goyal, S., Singh, O., & Panda, A. K. (1998). Stabilization of dichloromethane-induced protein denaturation during microencapsulation. *Pharmaceutical Development And Technology*, 3(2), 269-276.
34. Brange, J. (2000). Physical stability of proteins, in *Pharmaceutical Formulation Development of Peptides and Proteins* (eds S. Frokajer and L. Hovgaard), Taylor & Francis Limited, London, pp. 89–112.
35. Mozhaev, V. V., Khmel'nitskii, Y. L., Sergeeva, M. V., Belova, A. B., Klyachko, N. L., Levashov, A. V., & Martinek, K. (1989) *Eur. J. Biochem.* 184, 597.
36. Avanetto, F., B. Conti, I. Genta, & P. Giunchedi. (1992). Solvent evaporation, solvent extraction and spray drying for polylactide microsphere preparation. *Int. J. Pharm.* 84: 151–159.
37. Prathap, N. S., Min-chul, K., Fu-shi, Q., Martin, J. D., & Sang-Moo, K. Immunogenicity and Protection of Oral Influenza Vaccines Formulated into Microparticles. (2012). *Journal of Pharmaceutical Sciences*, Vol. 101, 3623–2635.
38. Uchida, T., A. Yagi, Y. Oda, & S. Goto. (1996). Microencapsulation of ovalbumin in poly (lactide-co-glycolide) by an oil-in-oil (o/o) solvent evaporation method. *J. Microencapsulation*. 13: 509–518.
39. Kumar, A. (2015). Development of Oral Influenza Vaccine Delivery System Utilizing pH Responsive Pored Microparticles. Thesis, University of Alberta.
40. Khan, M. Z., Prebeg, Z., & Kurjaković, N. (1999). A pH-dependent colon targeted oral drug delivery system using methacrylic acid copolymers. I. Manipulation Of drug release using Eudragit L100-55 and Eudragit S100 combinations. *Journal Of Controlled Release: Official Journal Of The Controlled Release Society*, 58(2), 215-222.
41. Chan, A., Orme, R. P., Fricker, R. A., & Roach, P. (2013). Remote and local control of stimuli responsive materials for therapeutic applications. *Advanced Drug Delivery Reviews*, 65(4), 497-514. doi:10.1016/j.addr.2012.07.007.
42. Foss, A. C., Goto, T., Morishita, M., & Peppas, N. A. (2004). Development of acrylic-based copolymers for oral insulin delivery. *European Journal Of Pharmaceutics And Biopharmaceutics: Official Journal Of Arbeitsgemeinschaft Fur Pharmazeutische Verfahrenstechnik E.V*, 57(2), 163-169.
43. Honey Priya, J., Rijo, J., Anju, A., & Anoop, K. (2014). Smart polymers for the controlled delivery of drugs – a concise overview. *Acta Pharmaceutica Sinica B*, Vol 4, Iss 2, Pp 120-127 (2014), (2), 120. doi:10.1016/j.apsb.2014.02.005

44. Pang X, Jiang Y, Xiao Q, Leung A, Hua H, Xu C. pH-responsive polymer-drug conjugates: Design and progress. *Journal Of Controlled Release: Official Journal Of The Controlled Release Society* [serial online]. January 28, 2016;222:116-129. Available from: MEDLINE, Ipswich, MA. Accessed April 15, 2017.
45. Kang, J., & Schwendeman, S. P. (2007). Pore closing and opening in biodegradable polymers and their effect on the controlled release of proteins. *Mol. Pharm.* 4, 104–118.
46. Liu, S., Cai, M., Deng, R., Wang, J., Liang, R., & Zhu, J. (2014). Fabrication of porous polymer microparticles with tunable pore size and density through the combination of phase separation and emulsion-solvent evaporation approach. *Korea Australia Rheology Journal*, 26(1), 63-71.
47. Miossec, P., Zkhiri, F., Pariès, J., David-Duflho, M., Devynck, M. A., & Valensi, P. E. (1999). Effect of pravastatin on erythrocyte rheological and biochemical properties in poorly controlled Type 2 diabetic patients. *Diabetic Medicine*, 16(5), 424–430. doi:10.1046/j.1464-5491.1999.00083.x
48. Jacobsen, W., Kirchner, G., Hallensleben, K., Mancinelli, L., Deters, M., Hackbarth, I., & Christians, U. (1999). Comparison of cytochrome P-450-dependent metabolism and drug interactions of the 3-hydroxy-3-methylglutaryl-CoA reductase inhibitors lovastatin and pravastatin in the liver. *Drug Metabolism and Disposition: The Biological Fate of Chemicals*, 27(2), 173–179.
49. Burger, C., Gerber, M., du Preez, J. L., & du Plessis, J. (2015). Optimised transdermal delivery of pravastatin. *International Journal of Pharmaceutics*, 496(2), 518–525. doi:10.1016/j.ijpharm.2015.10.034
50. Harisa, G. I., Badran, M. M., AlQahtani, S. A., Alanazi, F. K., & Attia, S. M. (2016). Pravastatin chitosan nanogels-loaded erythrocytes as a new delivery strategy for targeting liver cancer. *Saudi Pharmaceutical Journal: SPJ: The Official Publication Of The Saudi Pharmaceutical Society*, 24(1), 74–81. doi:10.1016/j.jsps.2015.03.024
51. Harisa, G. I., Ibrahim, M. F., & Alanazi, F. K. (2012). Erythrocyte-mediated delivery of pravastatin: in vitro study of effect of hypotonic lysis on biochemical parameters and loading efficiency. *Arch. Pharm. Res.* 35 (8), 1431–1439.
52. Kawabata, K., Samata, N., & Urasaki, Y. (2005). Quantitative determination of pravastatin and R-416, its main metabolite in human plasma, by liquid chromatography-tandem mass spectrometry. *Journal of Chromatography. B, Analytical Technologies in the Biomedical and Life Sciences*, 816(1–2), 73–79.

53. Whigan, D. B., Ivashkiv, E., & Cohen, A. I. (1989). Determination of pravastatin sodium and its isomeric metabolite in human urine by HPLC with UV detection. *Journal of Pharmaceutical and Biomedical Analysis*, 7(7), 907–912.
54. Otter, K., & Mignat, C. (1998). Determination of pravastatin in human plasma by high-performance liquid chromatography with ultraviolet detection. *Journal of Chromatography. B, Biomedical Sciences and Applications*, 708(1–2), 235–241.
55. Hyuk Im, S., Jeong, U., & Xia, Y. (2005). Polymer hollow particles with controllable holes in their surfaces. *Nature Materials*, 4(9), 671–675.
56. Rakhmatullin, I., Galiullina, L., Klochkova, E., Latfullin, I., Aganov, A., & Klochkov, V. (2016). Structural studies of pravastatin and simvastatin and their complexes with SDS micelles by NMR spectroscopy. *Journal Of Molecular Structure*, 110525-29. doi:10.1016/j.molstruc.2015.10.059
57. ¹H-NMR Spectrum of Sodium Lauryl Sulfate. https://www.drugbank.ca/spectra/nmr_one_d/2253